Ionic Conductivity and Exchange Current Density of Non-aqueous Lithium Polysulfide Electrolyte

By

Menghsuan Sam Pan

Submitted to the
Department of Materials Science and Engineering
In Partial Fulfillment of the Requirements for the Degree of

Bachelor of Science

at the

Massachusetts Institute of Technology

May 2015 [June 2015]

Signature of Author ..... Signature redacted
Department of Materials Science and Engineering
May 1, 2015

Certified by ..... Signature redacted
Yet-Ming Chiang
Kyocera Professor of Ceramics
Thesis Supervisor

Accepted by ..... Signature redacted
Geoffrey S.D. Beach
Associate Professor of Materials Science and Engineering
Chairman, Undergraduate Committee

Abstract

Lithium-polysulfide flow batteries, which utilize the high solubility of lithium polysulfide in non-aqueous electrolytes to enable flowable electrodes, have high theoretical energy density and low raw materials cost. To achieve greater electrode-level energy density, higher sulfur concentrations are needed. In a given electrolyte system, sulfur charge storage capacity (e.g. mAh/g sulfur) decreases dramatically with increasing sulfur concentration at a fixed C-rate, which corresponds to higher current output in higher concentration system. Understanding the limiting factors that undercut the rate capacity is crucial to enhancing the performance of high energy density systems. In particular, we systematically investigate the ionic conductivity and exchange current density at the electrode surface with lithium polysulfide solutions of varying concentration and in differing solvents which solvent molecules of different sizes. Ionic conductivities are measured using a commercially available conductivity probe, while exchange current densities are measured using both impedance spectroscopy and galvanostatic polarization using glassy carbon working electrodes.

The electrolyte solvent is found to dramatically affect the solution ionic conductivity and exchange current density. In the concentration range of interest (1-8 M [S]), the ionic conductivity monotonically decreases with increasing sulfur concentration while exchange current density shows a more complicated response in a given solvent system. Between solvent systems, we observed a five-fold increase in ionic conductivity, and a more than 15-fold enhancement in exchange current density. The conductivity and current density results are used to interpret the rate capability of suspension-based cells using lithium-polysulfide electrolyte and

carbon black as the cathode with different solvents. With the improvement in kinetics parameters, we also observed better rate capability in solvent. We also study non-carbonaceous electrode materials to understand how the electrode material can affect exchange current density and thus cell capacity. Indium tin oxide electrode shows lower exchange current density then glassy carbon electrode in preliminary results.

Table of Contents

List of Figures

List of Tables

List of Equations

1. Introduction

Grid-scale energy storage has raised interests in recent years as traditional electric grids currently operate very inefficiently. The fluctuating energy demand is met by varying electricity generation in real-time, and the intermittency limits the usage of renewable energies such as wind and solar powers. This requires the facilities to meet peak energy demands wasting large amount of capital on building and maintaining high capacity facilities as well as managing the power outputs [1]. At the same time, the overall electricity demand increases at an extremely fast rate (predicted to double by mid-century and to triple by the end of the century). The development of grid storage helps solve these problems by giving the grid the ability to shave the peak demands and shift the loads. In addition, storage improves the reliability and the stability of the grid by storing electricity locally. Moreover, grid storage can provide many other services such as frequency regulation and load following, cold start services, and contingency reserves [2]. However, grid-scale energy storage has not been implemented widely due to the insufficiency of energy storage technology. Scientists believe widespread grid storage application requires energy storage system with cost less than \$100 kWh^{-1} [3].

Electrochemical systems such as lithium-sulfur battery and lithium-air battery have been considered for grid-scale energy storage. Lithium-sulfur battery, in particular, has advantages of low cost and high theoretical energy density. Sulfur, the positive electrode material, costs as low as \$40 t^{-1} and has high theoretical capacity of 1675 mAh g^{-1} [4]. The soluble property of lithium polysulfide across a wide range of oxidation states (Li_2S_3 to Li_2S_8) in many organic solvents has inspired scientists to develop dissolved lithium polysulfides to be used as the cathode [5-8].

However, the technology suffers from several challenges including formation of insoluble non-conductive compounds and slow kinetics [9]. These challenges reduce the material utilization making the energy density much lower than the theoretical value especially in high concentration systems. Here, ionic conductivity and exchange current density of lithium polysulfide electrolyte are studied to understand the rate capability limitation.

2. Theoretical Background

2.1 Lithium-Sulfur Battery

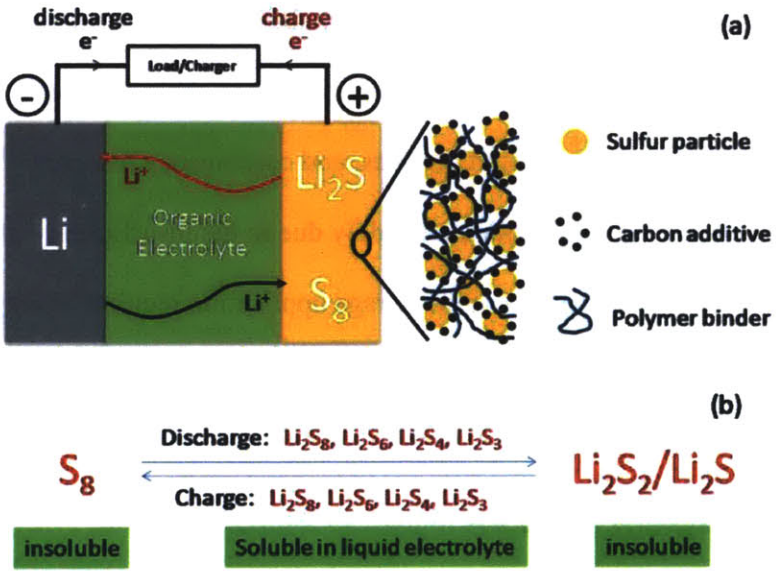

Figure 1: Conventional Lithium-Sulfur Battery [9]. Conventional Li-S battery consists of lithium metal anode, an organic electrolyte, and sulfur composite cathode. Operation of battery involves lithium-sulfur species of many oxidation states with Li_2S_3 to Li_2S_8 soluble in organic electrolyte solvent.

The sulfur-based positive electrode was first introduced by Herber and Ulam in 1962 [10], and Rao developed high-energy-density metal-sulfur batteries in 1966 [11]. After that, scientists focused more on the developing lithium-sulfur batteries primarily. The conventional Li-S battery, shown in figure 1, operates in a manner very similar to the lithium-ion battery. Reducing the cathode materials, in this cases sulfur, outputs energy, while lithium ions move through the electrolyte to maintain charge balance. Unlike a typical Li-ion battery, however, which only uses one or two oxidation states of the cathode, a Li-S battery involves multiple oxidization states (Li_2S_x for x form 1 to 8, and to S) [9]. Among these oxidation states, Li_2S_3 to Li_2S_8 are formed as species that dissolve in the electrolyte and can directly react chemically with the negative electrode, creating severe shuttle behavior and self-discharge effect. On the other hand, Li_2S and S, which are insoluble and non-conductive, form passivation layers resulting in low materials utilization, poor cycleability, and low energy efficiency [12].

In order to resolve these problems, scientists have taken various approaches [9, 13]. One of these takes advantage of lithium polysulfide solubility to design flowable electrodes for use in a flow battery. Flow batteries decouple the two electrodes by storing them in separate tanks away from reaction site helping to prevent self-discharge, and has inherent scalability since engineers can design the flow batteries such that the diffusive limit never constraint the performance of the batteries [5-8]. The scalability along with high energy density and low cost makes lithium-sulfur flow battery promising for grid-scale energy storage.

2.2 Electrical Double Layers

Electrical double layer (EDL) forms whenever an electrode or particle is immersed into an electrolyte solution. The surface develops surface charges, and then another equal and opposite charged layer form in the electrolyte to balance the charge. The formation of EDLs changes the particle-to-particle interaction because when the double layers overlap, the force can no longer be modeled by the simple Columbic force [14]. The electrical properties of the EDL affects the electrochemical measurements as well as the performance of the electrochemical system. The structure and the capacity of the double layer depend on the electrode materials, solvents, supporting electrolyte, and the species in the solution [15]. Since electrochemical reactions happen on the electrode-electrolyte interface, the exact composition and structure of the EDL affects the rate of these reactions. The EDL determines both the concentration of reactants at the interface and the rate that these particles move toward the interface [16].

2.3 Ionic Conductivity

The term conductivity associates with the particle flux under certain driving force. Ionic conductivity, here, describes the ion movements in electrolyte solution. Ionic flux under electric field driving force takes into account of both the ion mobility (proportional to ionic diffusivity by the Einstein relation) and concentration [17]. As a result, ionic conductivity can be expressed with equation 1.

Equation1: Ionic Conductivity

$$\sigma_{ionic} \propto c\,\mu$$

where σ_{ionic} is the ionic conductivity, c is the concentration, and μ is the ion mobility.

2.4 Butler-Volmer Relationship

The Butler-Volmer relation shown in figure 2 describes one of the most fundamental relationships that governs the charge transfer mechanism of the electrochemical reactions at the electrode surfaces. The relation shown in Equation 2 is valid when the electrode reaction rate is dominated by the charge transfer at the electrode-electrolyte interface instead of mass transfer. In the equation, the exchange current density i_0 describes the intrinsic rate of charge transfer of the electrochemical system [18]. To give an intuition, this value provides information about the difficulty for desired molecules to reach the reaction site and the reaction rate in Li-S batteries.

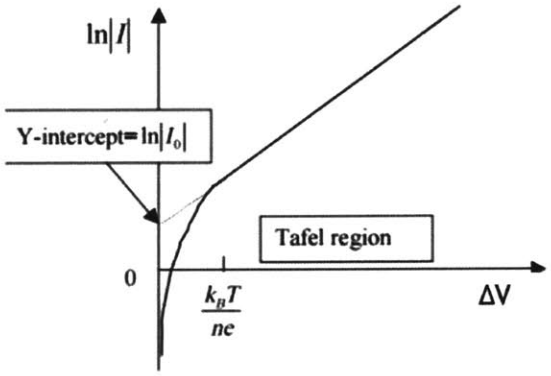

Figure 2: Butler-Volmer Relationship. The Tafel region represents the regime where charge-transfer limits the electrochemical reactions. Extrapolating the Tafel region to zero potential gives the exchange current.

According to the Bulter-Volnor equation, the current has an approximately exponential, or semi-logarithmic linear, dependence on overpotential when the absolute value of the overpotential is large. One of the exponential term goes to infinity, while the other goes to zero as absolute value

of the overpotential increases. Therefore, the exchange current density can be obtained by extrapolation of the linear Tafel region to zero overpotential. Essentially, the extrapolation drops one of the exponential term, and when the overpotential is set to zero, the value of the remaining exponential becomes one. Moreover, if the absolute values of the currents are ploted, the Tafel region extrapolations from positive current and negative current sizes intercept at exchange current density with zero overpotential.

Equation 2: Butler-Volmer Equation [18]

$$i = i_0 \left(e^{\frac{\alpha_a F \Delta V}{RT}} - e^{-\frac{\alpha_c F \Delta V}{RT}} \right)$$

where i is the current density, i_0 is the exchange current density, α_a is the cathodic charge transfer coefficient , α_c is the anodic charge transfer coefficient, F is the Faraday's constant, R is the gas constant, T is the temperature and ΔV is the overpotential.

3. Materials and Experimental Methods

3.1 Ionic Conductivity Measurement

Ionic conductivity governs the rate of ion movement in the electrolyte solutions. In other words, the term associates with the resistivity of the solution which affects both the kinetics of the batteries and the energy dissipation if mass transport is rate limiting. The ability for lithium ions to move across the solution from one electrode to the other limits the rate that electrons are extracted into the circuit and output energy. In this work, a portable ionic conductivity probe is used to measure the overall ionic conductivity of the electrolyte solutions.

3.2 Exchange Current Density Measurement

Another crucial kinetics parameter of electrochemical systems is the exchange current density, which measures the charge transfer limitation of the system. Two different methods of measuring exchange current density, electrical impedance spectroscopy and galvanostatic polarization, are utilized and compared.

3.2.1 Glassy Carbon Electrode Activation

The glassy carbon electrodes are commercially available but require activation before each measurement. Glassy carbon electrodes are first polished with alumina of 1 micron, 0.3 micron, and 0.05 micron average particle sizes in that order. After each polishing stage, the electrodes are rinsed with distilled water [19]. The polished electrodes are then dried in vacuum overnight before transferring into glove box for exchange current density measurements. Note that the activated electrodes are used in experiments within 24 hours of activation to ensure the accuracy of the result. To capture the effect of electrode deactivation exposed in argon and air, exchange current density measurements are performed versus the number of days after the electrode activations. Notable differences in exchange current density are only observed if electrodes are exposed to argon or air for more than a week.

3.2.2 Three-Electrode System

Three-electrode measurement, shown in figure 3(a), presents an accurate method to determine the current and potential difference of a given electrochemical system. Passing current through an electrode changes the potential measured, so segregating current and potential measurements allows more accurate measurements. In a three-electrode measurement, an ammeter, in series with the power supply, measures the current running from the working electrode to the counter electrode while the voltmeter measures the potential difference between the working electrode and the reference electrode [20]. No current runs from the working electrode to the reference electrode.

Here, the working electrodes are the potential candidate current collectors for lithium-sulfur batteries, glassy carbon and indium tin oxide (ITO), while the counter electrodes and reference electrodes are lithium metal. The glassy carbon electrodes are activated using the procedure describe in earlier section, and the ITO electrodes are prepared via sputter deposition onto stainless steel rods. The electrolyte solutions consist of various concentrations of lithium polysulfide Li_2S_6 ranging from 1 to 8 Molar (of sulfur) and 0.5 Molar lithium bis-trifluoromethanesulfonimide (LiTFSI) as solutes, and dioxolane/dimethoxyethane (DOL:DME = 1:1), diethylene glycol dimethyl ether (Diglyme), Triethylene glycol dimethyl ether (Triglyme), or Tetraethylene glycol dimethyl ether (Tetraglyme) as the solvent. An illustration of the three electrode system for lithium sulfur electrolyte solution is shown in figure 3(b). In the simplest term, this three electrode system essentially measures the potential required to activate the oxidation or reduction reaction of lithium polysulfide at a given rate.

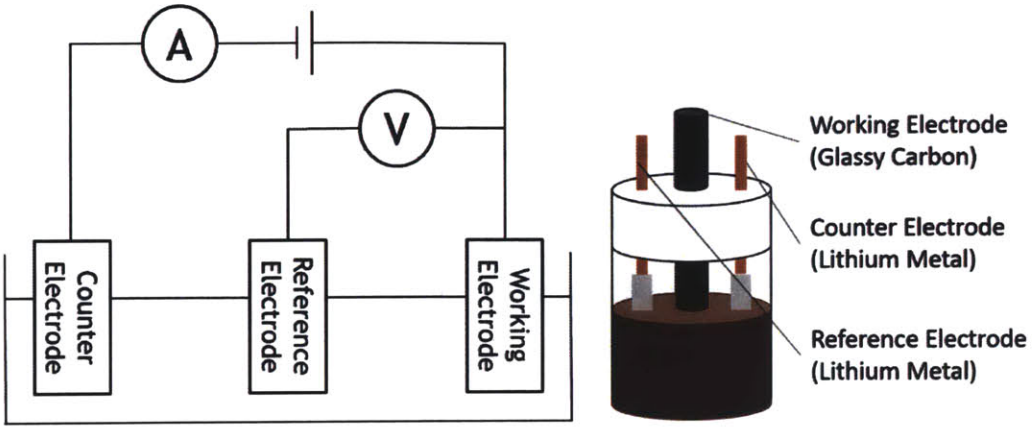

(a) (b)

Figure 3: Three-Electrode System. (a) Simple diagram representing the system. Ammeter, in series with the power supply, measures the current between working electrode and counter electrode, and the voltmeter measures the potential difference between the working electrode and the reference electrode. (b) In this project, the working electrode are glassy carbon or ITO while the counter electrode and the reference electrode are lithium metal.

3.2.3 Electrochemical Impedance Spectroscopy

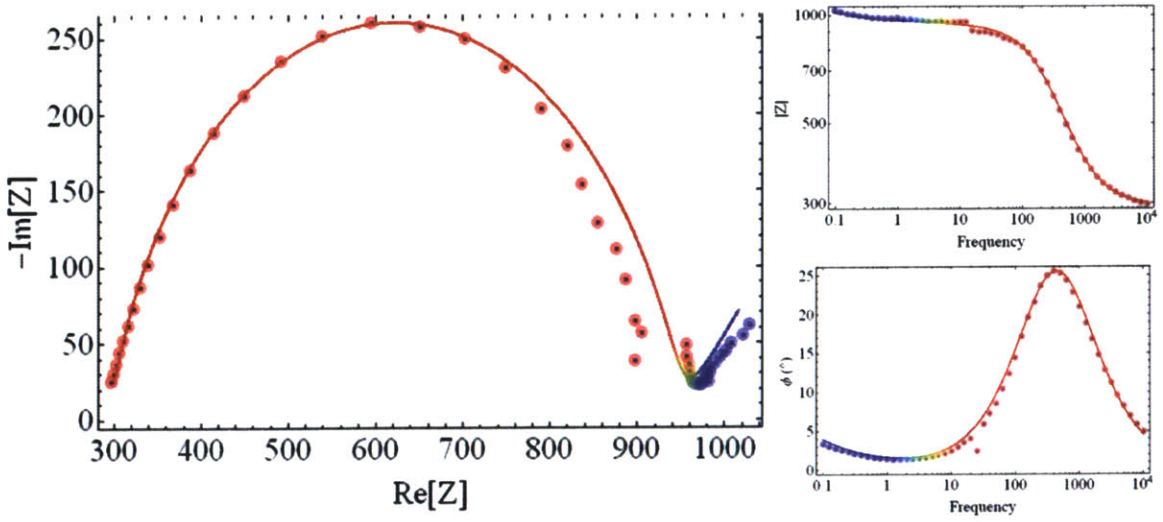

Figure 4: Electrochemical Impedance Spectroscopy. The real impedance represents the resistance term of the circuits, while the negative imaginary impedance represents the capacitance. The magnitude of the real impedance is the amplitude ratio of the voltage input and the current response, and the angle is determined by the phase lag of the potential and current. The charge transfer resistance and the exchange current density are calculated from the width of the arc.

The first method of measuring exchange current density uses electrochemical impedance spectroscopy (EIS). EIS measurement applies alternating voltage signal and measures the phase shift between the current signal and the voltage signal to extract the capacitance or inductance properties. With this idea, for each given frequency of AC signal, the magnitude of impedance response is the ratio of the voltage amplitude and current amplitude (note the unit is equivalent to that of resistance), while the angle maps to the phase lag of current with respect to the voltage input. The measured data is then expressed by complex impedance with real part representing resistance, positive imaginary part representing inductance, and negative imaginary part representing capacitance [21].

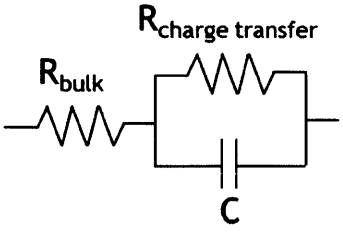

Figure 5: Circuit Equivalence. The three electrode systems in this work map to this equivalent circuit. The bulk resistance accounts for the solution resistance and metal resistance. The charge

transfer resistance describes the rate that reaction can happen on the current collector surface, and the capacitance term describes the charge buildup at the electrolyte-collector interface.

In lithium sulfur batteries, the exchange current density directly relates to charge transfer resistance, which has capacitance characteristic as charges build up at the electrolyte-current collector interface while batteries are operating. This capacitance characteristic allows the EIS to effectively separate charge transfer resistance from the bulk resistance by looking at the imaginary impedance. As a result, the impedance data is fitted to a simple circuit equivalence shown in figure 5 which has a typical impedance response shown in figure 4 to obtain the charge transfer resistance. The capacitor acts as a short circuit at high frequencies and acts as an open circuit at low frequencies due to the capacitor responses to charge buildup, so the high frequency limit of the equivalent circuit is just the bulk resistance, while the low frequency limit of the equivalent is the bulk resistance plus the charge-transfer resistance. In the case, the charge transfer resistance is the width of the arc in the impedance plot. Equation 3 then relates the charge transfer resistance to exchange current density.

Equation 3: Modified Nernst Equation [18]

$$i_0 = \frac{RT}{nFR_{charge-transfer}A}$$

where i_0 is the exchange current density, R is the gas constant, T is the temperature, n is the number of charge per ion, F is the Faraday's constant, $R_{charge\text{-}transfer}$ is the charge transfer resistance, and A is the active area of the current collector.

3.2.4 Galvanostatic Polarization

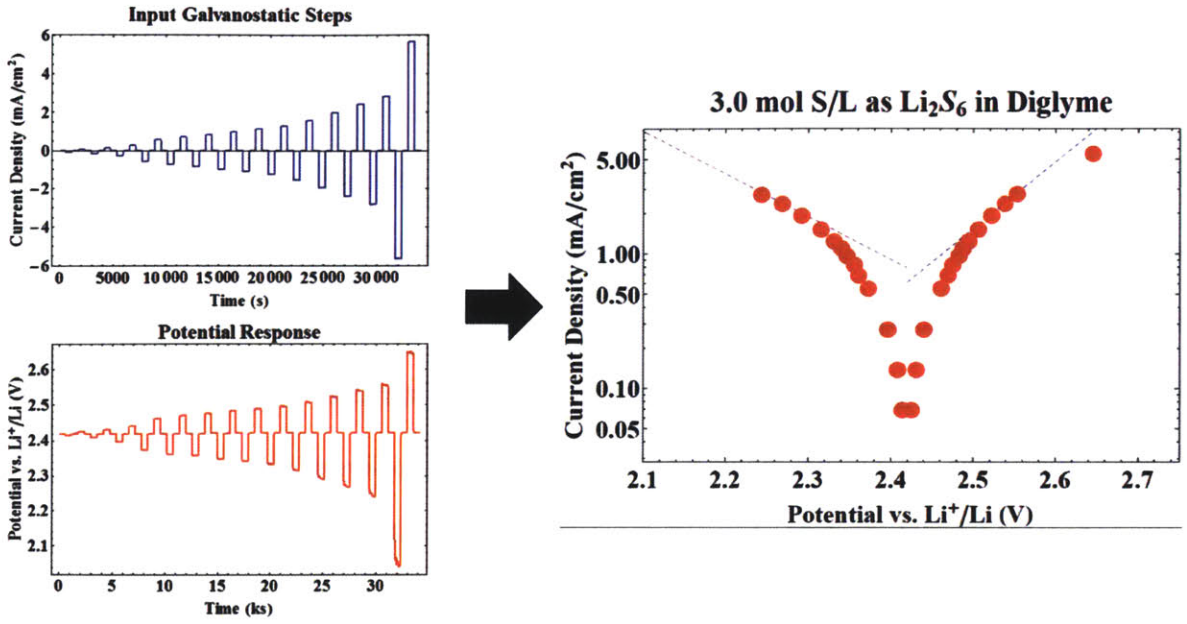

(a) (b)

Figure 6: Galvanostatic Polarization and Tafel Plot. The current step input and potential response pairs form the Tafel plot on the right. The semi-logarithmic linear regimes of the Tafel are governed by the charge transfer limitations and Butler-Volmer relation, and their interaction represents the equilibrium potential and exchange current.

The second method uses galvanostatic polarization along with knowledge on charge transfer theory. Galvanostatic polarization applies various constant positive and negative current inputs over a certain period of time to obtain stable potential responses shown in figure 6(a). Tafel plots are then constructed with these currents' absolute value and potential pairs for a given system. The Tafel plot plots the current in logarithmic scale on the vertical axis and the potential in linear scale on the horizontal axis as shown in figure 6(b). The Butler-Volmer relationship is applied to the semi-logarithmic linear regime of the Tafel plots in which the system limits by the charge transfer at the interfaces. The interception of the extrapolated linear regimes of positive currents

and negative currents gives the equilibrium potential and the exchange current, which is then normalized to exchange current density with respect to active area of the current collector.

3.3 Battery Capacity Measurement

The kinetics parameters help to understand the fundamental science and limiting factors of batteries, but they do not provide information about the usability of batteries. Ultimately, society cares about the capacity and the energy efficiency of the batteries. Therefore, measuring how the kinetics properties affects the rate capability links this work to the practical aspect of batteries. In general, the energy efficiency and capacity drops with increasing charge and discharge rate since more energies are used to overcome the kinetic resistance. By convention, the charge and discharge rate are expressed in term of C rates, in which 1C represents complete charged or discharged over 1 hour while C/5 represents over 5 hours.

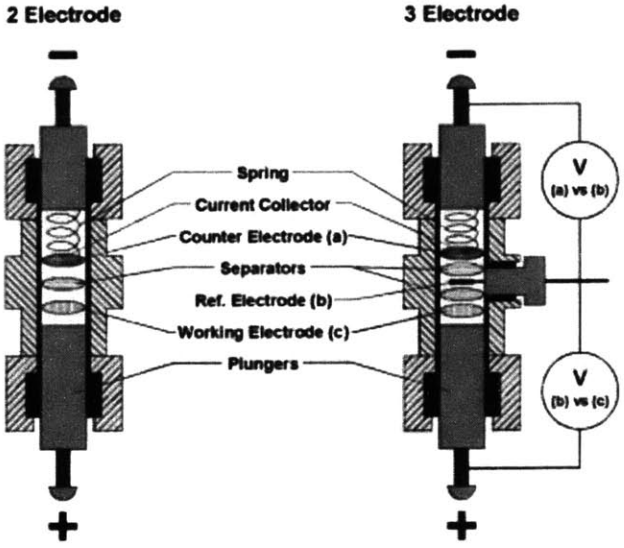

Figure 7: Swagelok Cell [22]. The lithium-polysulfide suspensions are used as the cathode (working electrode) in 2-electrode Swagelok cells which then undergo capacity test to obtain the materials utilization with a specific charge/discharge rate.

Carbon black powders are mixed into lithium sulfur electrolyte solution to enhance the electrical conductivity. The resulting suspension is then used as the cathode in a 2-electrode Swagelok cell shown in figure 7 with lithium metal as the anode and a porous polymer separator between the electrodes. Then, the cell undergoes constant current input corresponded to a desired C rate and the voltage responses are measured until the batteries can no long output any energy. This way, the total runtime corresponds to the capacity and materials utilization while the current-voltage relation allows the calculation of total energy output.

4. Results and Discussion

4.1 Ionic Conductivity

In the sulfur concentration range of interest (1-8 Molar), ionic conductivity decreases monotonically with increasing sulfur concentration in all solvent systems. The result for the ionic conductivity measurements are shown in figure 8. However, there exists no single simple function that describe the decreasing trend for all solvent systems. When considering the ionic conductivity of a single solvent, there are two opposite trends associated with increasing solute concentration: the amount of ions available in the solution and the mobility of individual ions. Obviously, the more lithium polysulfide dissolved the more ions available. On the other hand,

the mobility decreases with sulfur concentration because of the "crowdedness" rises with concentration. Since molecules have volume and mass, larger number of surrounding molecules make it harder to move through them. In the experiments, higher viscosity is also observed for higher sulfur concentration, which further supports this explanation. Combining the two trends, the ionic conductivity is expected to increase initially as the increasing ion concentration dominates the trend and start to drop after peaking as the decaying mobility takes over. This also fits the observations that the ionic conductivity dropping rate increases in some systems (DOL:DME and diglyme) but decreases in others (triglyme and tetraglyme).

Comparing the ionic conductivity across different solvent systems at any given sulfur concentration, the DOL:DME system (5x of tetraglyme system) has the highest ionic conductivity, then diglyme, triglyme, and finally, tetraglyme. The different ethers have the same functional group interacting similarly with molecules and ions, and differ only in molecule chain lengths, so the effect must come from the size differences. The chain length of the solvent molecules inversely correlates with the ionic conductivity. Again, ionic conductivity takes into account the concentration of ions available and the mobility of the ions. The concentration of ions in the solution remains the same since the same sulfur concentrations are discussed. However, the mobility of the ions changes from one solvent system to another because larger solvent molecules create larger resistivity for ions movement. In experiment, the longer molecule systems exhibit higher viscosity clearly ranging from water like texture (DOL:DME) to ketchup like texture (tetraglyme), and thus lower mobility according to the Stokes-Einstein equation shown in Equation 4.

Equation 4: Stokes-Einstein Equation

$$D = \mu k_B T = \frac{k_B T}{6 \pi \eta r}$$

where D is the diffusion constant, μ is the mobility, k_B is the Boltzmann's constant, T is the temperature, η is the viscosity, and r is the radius of the particle.

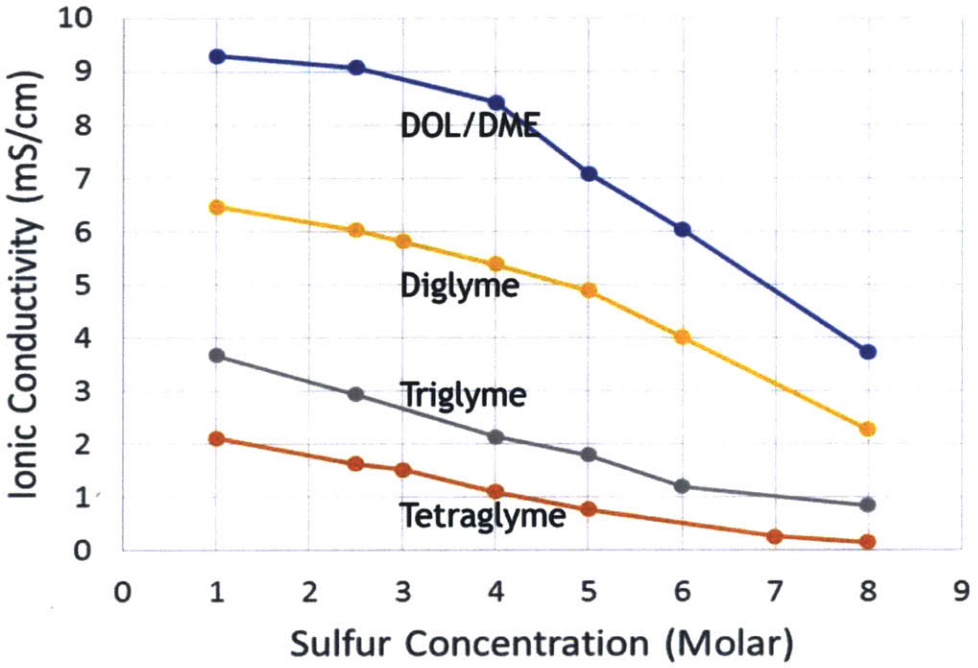

Figure 8: Ionic Conductivity of Various Solvent Systems. Ionic conductivity decreases monotonically with concentration and solvent molecule size. In any given sulfur concentration, DOL:DME system has the highest ionic conductivity while tetraglyme has the lowest.

4.2 Exchange Current Density

4.2.1 Electrochemical Impedance Spectroscopy versus Galvanostatic Polarization

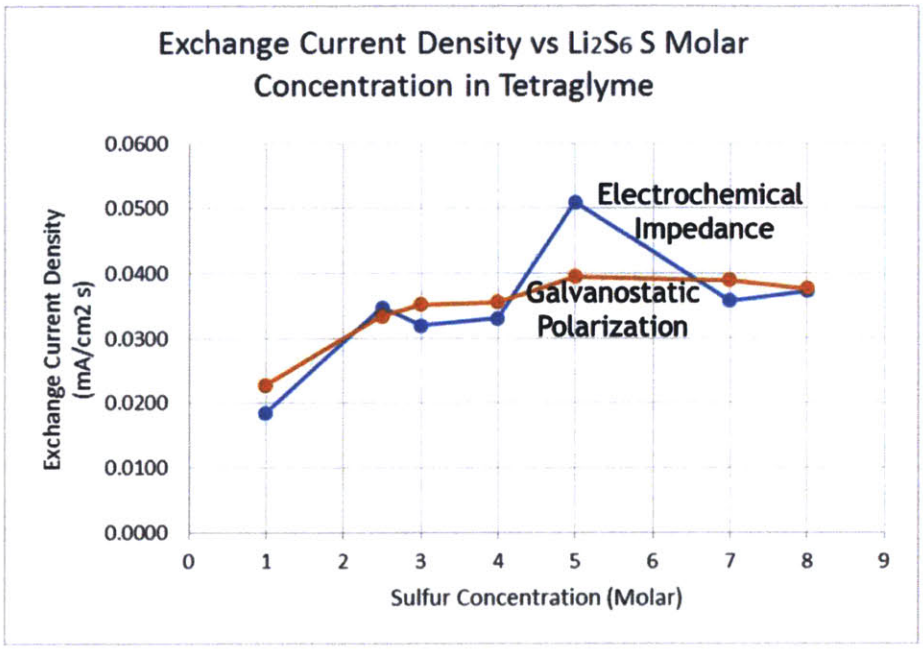

Figure 9: Exchange Current Density in Tetraglyme. Galvanostatic polarization generates more precise data but electrochemical impedance measurement is less time consuming.

The results for tetraglyme system two measurement techniques for which the results for tetraglyme system are shown in figure 9 have different advantages and disadvantages. Electrochemical impedance spectroscopy (EIS) provides a time conserving and convenient way to measure exchange current densities. In volatile solvent systems such as DOL:DME system, galvanostatic polarization is unfeasible with open cells as the experiments require more than twenty hours, while EIS takes less than twenty minutes. The DOL:DME system experiences observable evaporation over twenty hours which alters the results of the measurements as concentration varies over time. However, EIS is subject to larger trial to trial deviation. In this work, the results for EIS experience up to 2-fold difference even though the chemicals and experiments are prepared and setup identically. On the other hand, galvanostatic polarization,

although takes a long time, shows very little trial to trial deviations. Therefore, in contrast to EIS, galvanostatic polarization has characteristic of higher precision although it is more time consuming. For detail EIS and galvanostatic polarization data and analysis, please see Appendix 1 and 3.

4.2.2 Concentration Effect

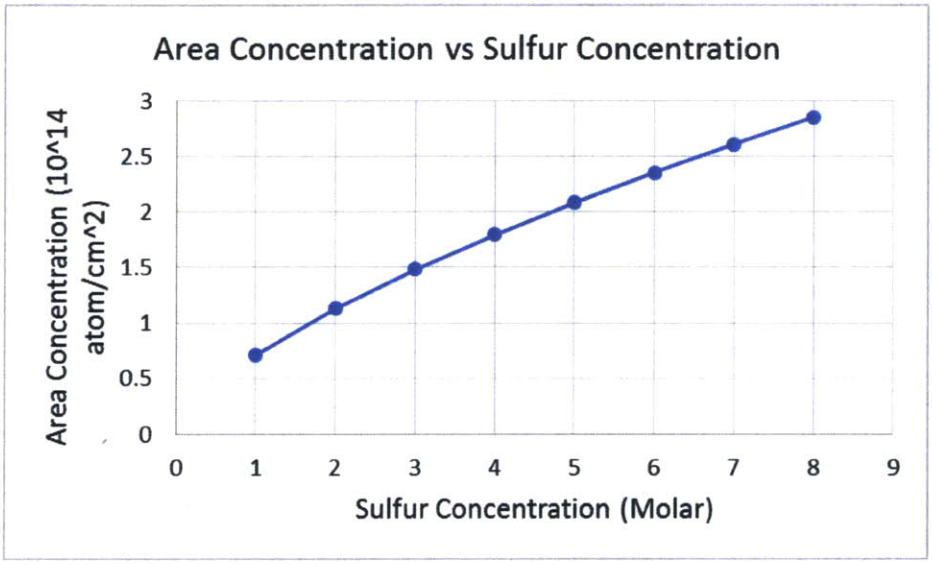

Figure 10: Area Concentration Versus Sulfur Concentration. Area concentration show slightly slower dependence on sulfur concentration than linear dependence. This dependence on sulfur concentration is very similar to that of ionic conductivity in diglyme and triglyme systems.

The exchange current densities of different solvent systems show different and complicated dependences on concentration. Exchange current density corresponds to the charge transfer limitation, which relates to the reaction rate and the reactant concentration at the electrode-electrolyte interface. Within the same solvent system, the reaction rate should not change as the

reactants and environments remain the same. In dilute solutions, the solute molecules and ions are well separated such that their movements and electric double layers do not intervene with each other. Exchange current density then should increase almost linearly with bulk concentration since area concentration at the interface scales with the bulk concentration as shown in figure 10 when electrical field drives ions and molecules toward the interface. The exchange current densities of the diglyme system and triglyme system do show very similar dependences on concentration as shown in figure 11(b, c). The molecules and ions in these solvent systems barely interact with each other because the electric double layers are not thick enough to overlap with each other in the sulfur concentration interested.

However, the exchange current density of tetraglyme system shown in figure 11(a) exhibits a more complicated trend than linear with a nearly constant value beyond 3M. In this case, the dilute solution assumption does not hold. The polar solvent molecules along with other ions in the solution form the electric double layers, and the double layer thickness increases as the solvent molecule size increases. This means, in tetraglyme system, the dilute solution assumption fails at a lower concentration than other solvent systems. At high concentration, the electric double layers overlap with each other forming intermolecular forces among the double layer molecules. In order for the electrochemical reaction to occur, the lithium ions and polysulfide molecules need to break through the double layers to reach the electrode. But the energy required to break these double layers increases due to the double layers interactions reducing the exchange current density. As a result, the exchange current density no longer has a linear dependence on the sulfur concentration. In fact, the exchange current density peaks at some

intermediate concentration and starts dropping because the energy required to reach the interface becomes so high that this energy limits the exchange current density.

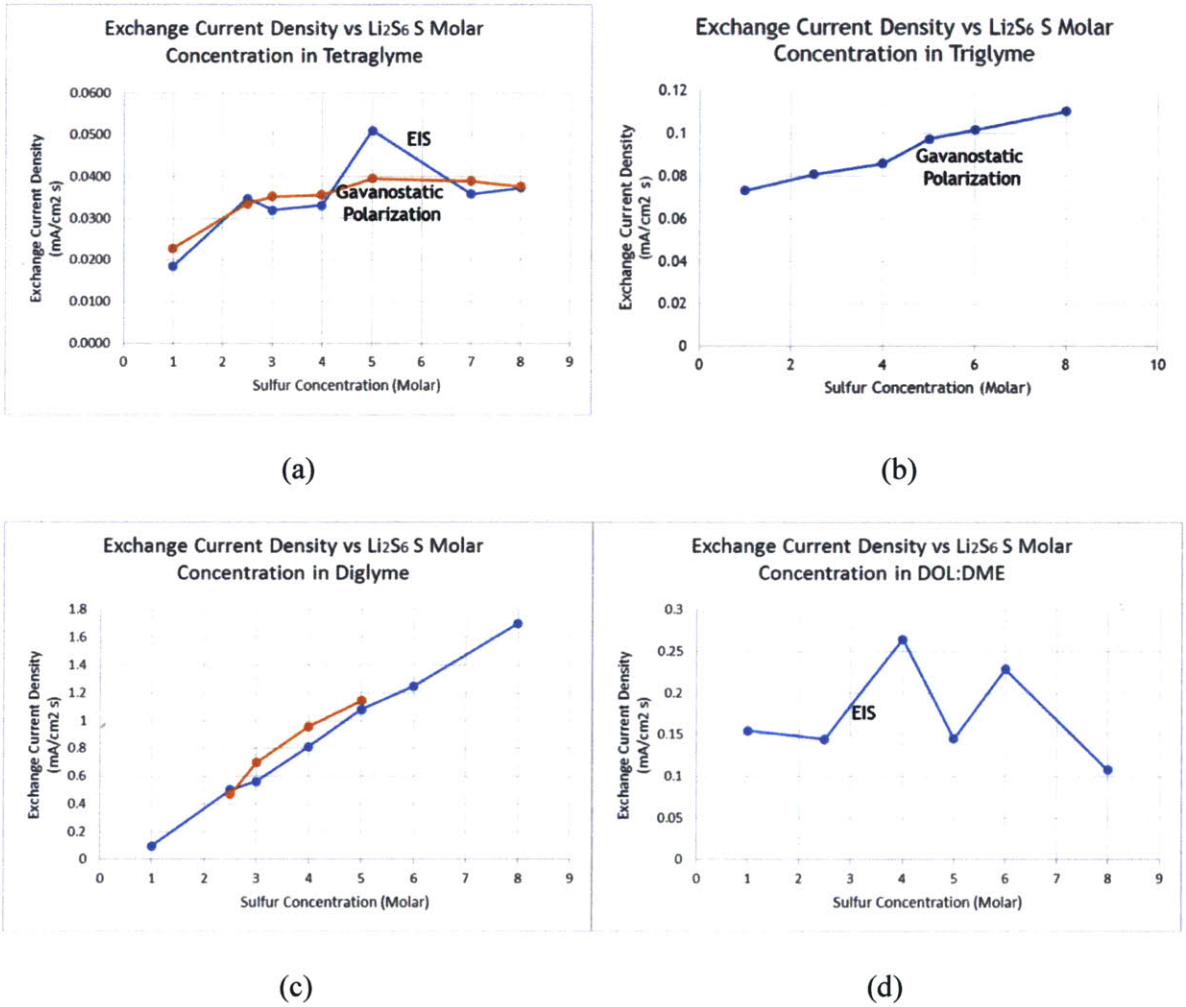

Figure 11: Exchange Current Density vs Sulfur Concentration. Exchange current density in different solvent system exhibit different dependence on sulfur concentration. There is an almost linear dependence in triglyme and diglyme systems while there exists a more complicated dependence in tetraglyme system with a maximum at 5 Molar sulfur concentration.

Finally, for DOL:DME system, only EIS measurements can be performed due to the high volatility of the solvent. The results shown in figure 11(d) experience large amount of errors such that no conclusion in concentration dependence can be drawn.

4.2.3 Solvent Effect

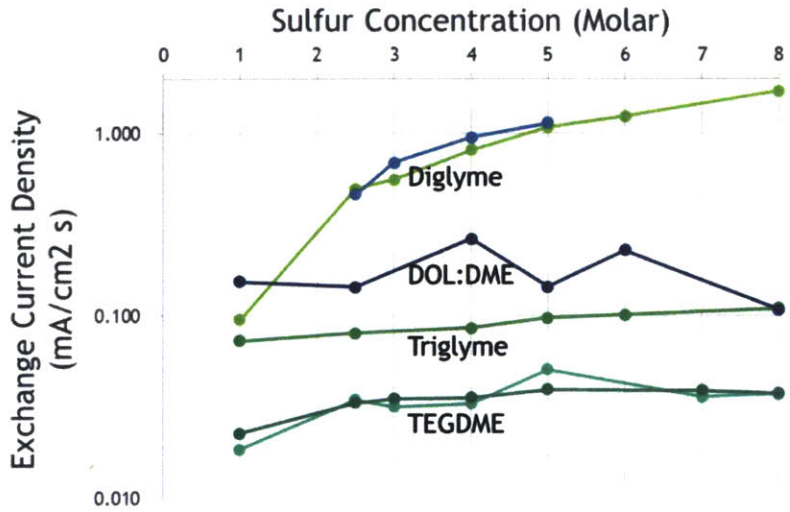

Figure 12: Exchange Current Density Comparison. Exchange current density increases as the solvent molecule chain length gets shorter in solvent molecules of same chemistry. DOL:DME system, however, shows a lower exchange current density then diglyme system at high sulfur concentration. From tetraglyme to diglyme system, there exists a fifteen-fold increase in exchange current density.

Just like ionic conductivity, exchange current density increases as solvent molecule sizes decreases in tetraglyme, triglyme, and diglyme systems as shown in figure 12. The size of molecule affects the electrical double layers of the ions and molecules as well as the electrode.

The thicker double layers are expected to require more energy to break through. This means the thicker the double layer, the lower the exchange current density, which agrees with the results. On the other hand, DOL:DME system has exchange current densities lower than that of diglyme even though DME molecules are smaller than diglyme molecules. As mention earlier, the composition and the structure of the double layer depend on not only the size of solvent molecules but also the chemistry of solvent. It is unclear how the addition of DOL, which has different functional group than any other solvents used, will affect the double layer. To understand the exact effect of DOL, additional experiments on DME as solvent or DOL:triglyme as solvent are required. Nevertheless, the exchange current density is increased by more than 15-fold from tetraglyme to diglyme system.

4.2.4 Glassy Carbon versus ITO Electrode

Electrode	Glassy Carbon	ITO
.5M in Triglyme	0.097 mA/cm2	0.022 mA/cm2

Table 1: Exchange Current Density of Glassy Carbon and ITO electrodes. Glassy carbon electrode shows allows a much higher exchange current density than ITO electrode.

The electrode materials can also alters the structure and composition of the electrical double layer. Here, glassy carbon electrodes and ITO electrodes are used. As shown in table 1, glassy carbon electrode has a much higher (more than 4 times) exchange current density that that of ITO electrode.

4.3 Cell Capacity

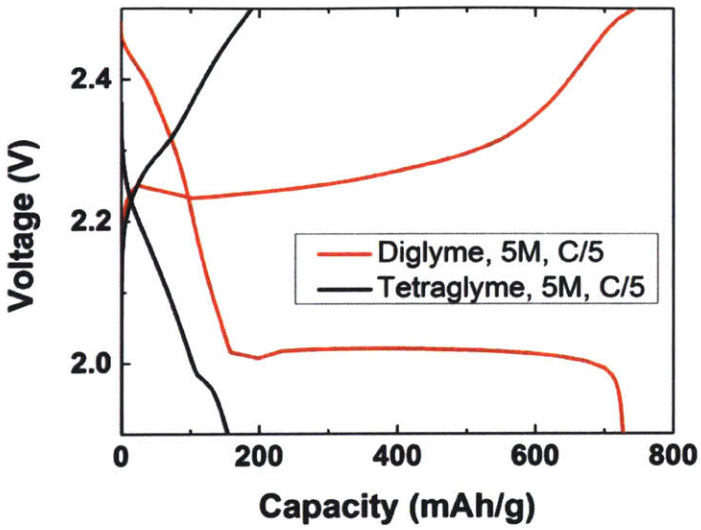

Figure 13: Cell Capacity of Tetraglyme and Diglyme System at C/5 Rate. At C/5 rate, diglyme system has a 5-fold increase from tetraglyme system.

Tetraglyme has been widely used as the electrolyte solvent in Li-S batteries, but the cell capacity suffers even at a rate of C/5 charge/discharge rate. Cells using tetraglyme as electrolyte solvent has a capacity of around 150 mAh g^{-1} S which is far from the theoretical energy density of 1675 mAh g^{-1}. This means the material utility in that particular experiment is less than 10 percent. To understand how the kinetic parameters affect the rate capability, cell capacity test of the same rate using diglyme as the electrolyte solvent was performed. The cells have capacities of more than 700 mAh g^{-1} S, 5 times more than cells using tetraglyme as shown in figure 13. Although the material utility is still less than 50 percent, but the promising results proves that enhancing the kinetics parameters helps the rate capability. Therefore, the changing the electrolyte solvent does improve the rate capability of Li-S battery.

5. Conclusion

In non-aqueous lithium-polysulfide electrolytes, both sulfur concentration and solvent effect the ionic conductivity and exchange current density dramatically. In the concentrations of interest, ionic conductivity decreases as concentration increases and increases as glyme solvent molecules gets smaller due to the mobility changes. Exchange current density, however, shows much more complicated responses to concentration and solvent. Nevertheless, a 5-fold increase in ionic conductivity and a 15-fold improve in exchange current density are observed in the solvent systems we have tried. These enhancements in kinetics parameters resulted in an improved rate capability in suspension-based batteries. Although the rate capability and materials utilization have not reached the desired value, and the capacities fall far short of the theoretical value, this result has shown that improving the ionic conductivity and exchange current density and changing the solvent do improve the practicality of the Li-S batteries. In term of solvent, the goal for the future will be searching for solvents that further improves the kinetics parameters and thus the rate capability.

In addition to solvent, the electrode material also influences the exchange current density. Here, we have obtain preliminary data comparing glassy carbon electrode and ITO electrode showing that glassy carbon electrode is a much more favorable electrode. However, the exact mechanism of how electrode materials affect the exchange current density remain unrevealed. Therefore, performing more experiments and characterizations on glassy carbon electrodes and ITO electrodes are necessary to systematically improve the kinetics from the electrode point of view.

6. Acknowledgement

This work was supported as part of the Joint Center for Energy Storage Research, an Energy Innovation Hub funded by the U.S. Department of Energy, Office of Science, Basic Energy Sciences. The author thanks Prof. Yet-Ming Chiang for the technical instructions and materials science knowledge inputs, and Dr. William Woodford and Mr. Frank Fan for laboratory trainings and instructions. Also, Mr. Frank Fan deposited the indium tin oxide electrodes and ran the cell capacity experiments presented in this work, and Prof. Craig Carter provides the Mathematica code for fitting the electrochemical impedance spectroscopies and linear regimes of the Tafel plots.

References

[1] Dunn, B., Kamath, H., & Tarascon, J. (2011). Electrical Energy Storage for the Grid: A Battery of Choices. Science, 334, 928-935.

[2] Yang, Z., Zhang, J., Kintner-Meyer, M., Lu, X., Choi, D., Lemmon, J., & Liu, J. (2011). Electrochemical Energy Storage for Green Grid. Chemical Reviews, 111, 3577-3613.

[3] "ARPA-E FOA# DE-FOA-0000290: Grid-Scale Rampable Intermittent Dispatchable Storage (GRIDS)," https://arpa-e-foa.energy.gov/FoaDetailsView.aspx?foaId=85e239bb-8908-4d2c-ab10-dd02d85e7d78

[4] Bruce, P., Freunberger, S., Hardwick, L., & Tarascon, J. (2011). Li–O2 and Li–S batteries with high energy storage. Nature Materials, 172-172.

[5] Yang, Y., Zheng, G., & Cui, Y. (2013). A membrane-free lithium/polysulfide semi-liquid battery for large-scale energy storage. Energy & Environmental Science, 6, 1552-1558.

[6] Demir-Cakan, R., Morcrette, M., Guéguen, A., Dedryvère, R., & Tarascon, J. (2013). Li–S batteries: Simple approaches for superior performance. Energy & Environmental Science, 6, 176-182.

[7] Rauh, R., Abraham, K., Pearson, G., Surprenant, J., & Brummer, S. (1979). A Lithium/Dissolved Sulfur Battery With An Organic Electrolyte. Journal of The Electrochemical Society, 126(4), 523-527.

[8] Fan, F. Y., Woodford, W. H., Li, Z., Baram, N., Smith, K. C., Helal, A., McKinley, G. H., Carter, W. C., & Chiang, Y.-M. (2014). Polysulfide Flow Batteries Enabled by Percolating Nanoscale Conductor Networks. Nano Letters, 14(4), 2210–2218-2210–2218.

[9] Manthiram, A., Fu, Y., & Su, Y. (2013). Challenges and Prospects of Lithium–Sulfur Batteries. Accounts of Chemical Research, 46(5), 1125-1134.

[10] Danuta, H, and Ulam J. Electric Dry Cells and Storage Batteries. Electric Tech Corp, assignee. Patent US3043896 A. 26 Nov. 1957. Print.

[11] Rao, M. L. B. Organic Electrolyte Cells. Mallory & Co Inc P R, assignee. Patent US3413154 A. 23 Mar. 1968. Print.

[12] Manthiram, A., Fu, Y., Chung, S., Zu, C., & Su, Y. (2014). Rechargeable Lithium–Sulfur Batteries. Chemical Reviews, 114, 11751-11787.

[13] Evers, S., & Nazar, L. (2013). New Approaches for High Energy Density Lithium–Sulfur Battery Cathodes. Accounts of Chemical Research, 46(5), 1135-1143.

[14] Attard, P. (1996). Electrolytes and the Electric Double Layer. Advances in Chemical Physics, 92, 1-159.

[15] Stojek, Z. (2010). The Electric Double Layer and Its Structure. In F. Scholz (Ed.), Electroanalytical methods guide to experiments and applications (2nd, rev. and extended ed.). Heidelberg: Springer.

[16] Inzelt, G. (2010). Kinetics of Electrochemical Reactions. In F. Scholz (Ed.), Electroanalytical methods guide to experiments and applications (2nd, rev. and extended ed.). Heidelberg: Springer.

[17] Bockris, J., & Reddy, A. (2002). Modern electrochemistry (2nd ed.). New York: Kluwer Academic.

[18] Newman, J. (1972). Electrochemical systems (3rd ed.). Englewood Cliffs, N.J.: Prentice-Hall.

[19] Dekanski, A., Stevanovic, J., Stevanovic, R., Nikolic, B., & Jovanovic, V. (2001). Glassy carbon electrodes: I. Characterization and electrochemical activation. Carbon, 39, 1195-1205.

[20] Bard, A., & Faulkner, L. (1980). Electrochemical methods: Fundamentals and applications. New York: Wiley

[21] Alexander, C., & Sadiku, M. (2007). Fundamentals of electric circuits (3rd ed.). Boston: McGraw-Hill Higher Education.

[22] Amatucci, G., Badway, F., Pasquier, A., & Zheng, T. (2001). An Asymmetric Hybrid Nonaqueous Energy Storage Cell. Journal of The Electrochemical Society, 148(8), A930-A939.

Appendix

Appendix 1. Electrochemical Impedance Spectroscopy for Varying Concentration in Different Solvent System

1.1 Electrochemical Impedance Spectroscopy Tetraglyme

1.1.1 Electrochemical Impedance Spectroscopy Tetraglyme 1 Molar Sulfur

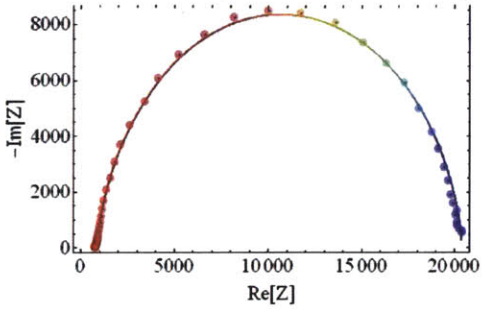

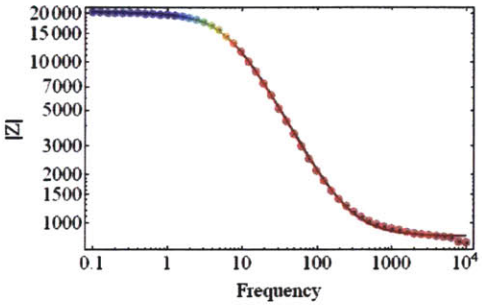

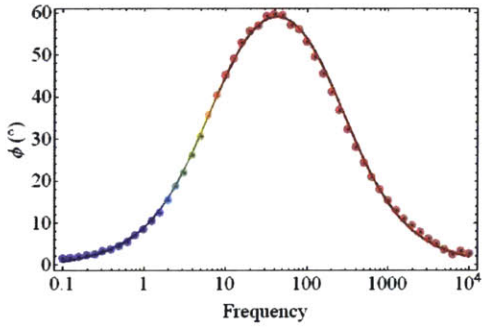

Log_{10} Norm Distance = 0.908
Solution Resistance = 823.902
Warburg (Ohm $s^{-1/2}$) −60.127
Charge−Transfer Resistance (Ohm) 19759.152
CPE exponent 0.896
CPE Capacitance (μF) 8.759

1.1.2 Electrochemical Impedance Spectroscopy Tetraglyme 2.5 Molar Sulfur

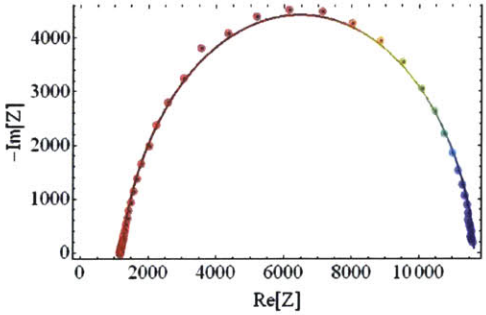

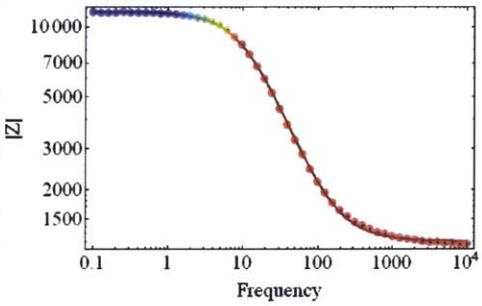

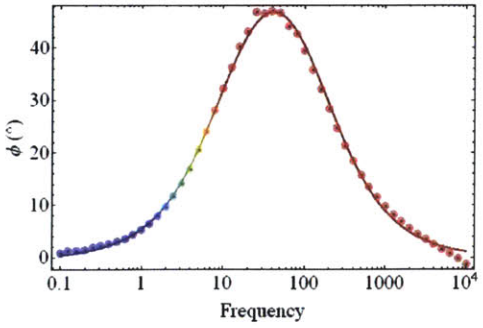

Log_{10} Norm Distance = −0.581
Solution Resistance = 1204.274
Warburg (Ohm $s^{-1/2}$) −29.709
Charge−Transfer Resistance (Ohm) 10539.178
CPE exponent 0.891
CPE Capacitance (μF) 10.774

1.1.3 Electrochemical Impedance Spectroscopy Tetraglyme 3 Molar Sulfur

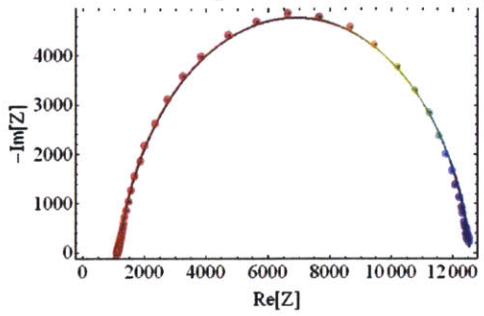

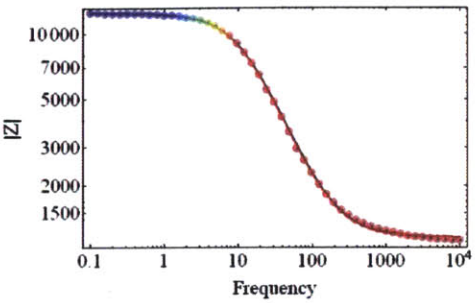

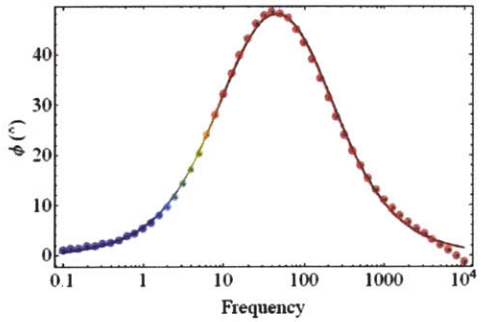

Log_{10} Norm Distance = −0.573
Solution Resistance = 1157.032
Warburg (Ohm $s^{-1/2}$) −16.287
Charge−Transfer Resistance (Ohm) 11468.171
CPE exponent 0.884
CPE Capacitance (μF) 9.894

1.1.4 Electrochemical Impedance Spectroscopy Tetraglyme 4 Molar Sulfur

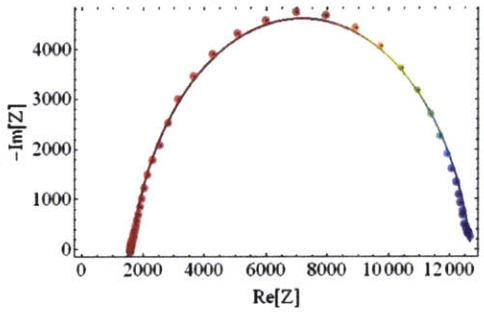

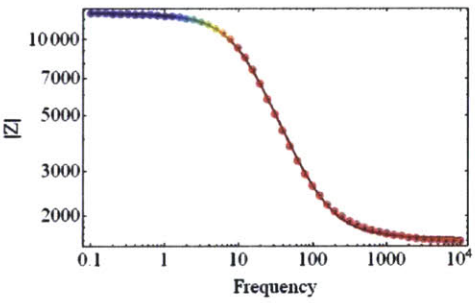

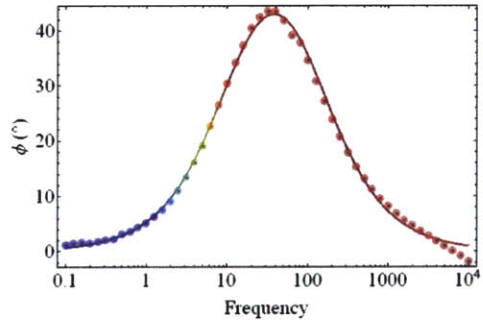

Log_{10} Norm Distance = −0.587
Solution Resistance = 1625.489
Warburg (Ohm $s^{-1/2}$) −2.256
Charge−Transfer Resistance (Ohm) 11074.115
CPE exponent 0.885
CPE Capacitance (μF) 10.155

1.1.5 Electrochemical Impedance Spectroscopy Tetraglyme 5 Molar Sulfur

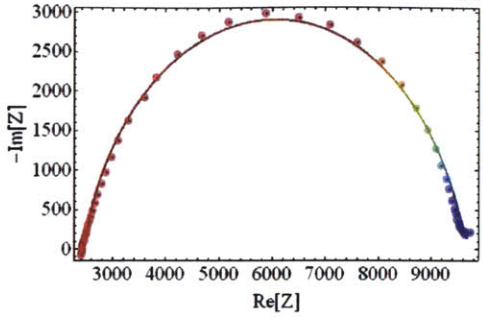

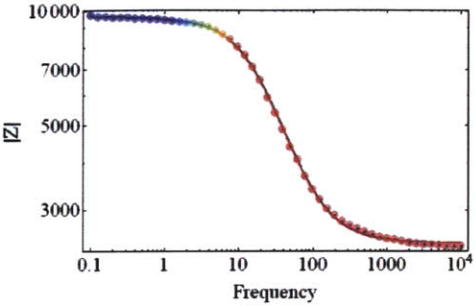

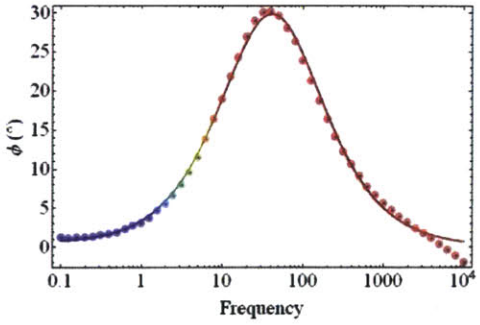

Log_{10} Norm Distance = −0.519
Solution Resistance = 2455.697
Warburg (Ohm $s^{-1/2}$) 29.254
Charge−Transfer Resistance (Ohm) 7184.564
CPE exponent 0.866
CPE Capacitance (μF) 11.059

1.1.6 Electrochemical Impedance Spectroscopy Tetraglyme 7 Molar Sulfur

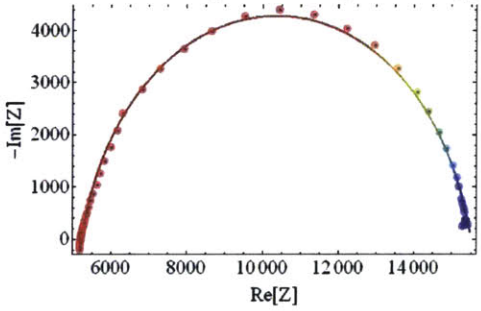

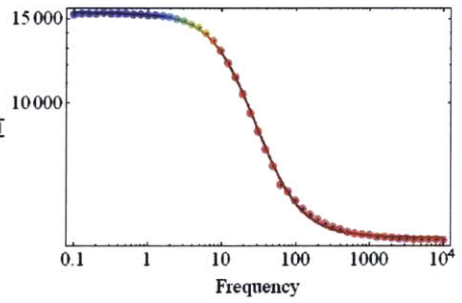

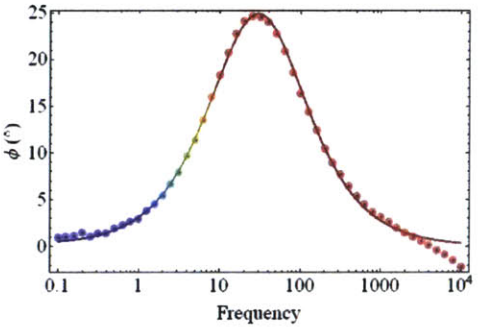

Log_{10} Norm Distance = −0.488
Solution Resistance = 5249.227
Warburg (Ohm $s^{-1/2}$) 13.435
Charge−Transfer Resistance (Ohm) 10228.203
CPE exponent 0.887
CPE Capacitance (μF) 8.292

1.1.7 Electrochemical Impedance Spectroscopy Tetraglyme 8 Molar Sulfur

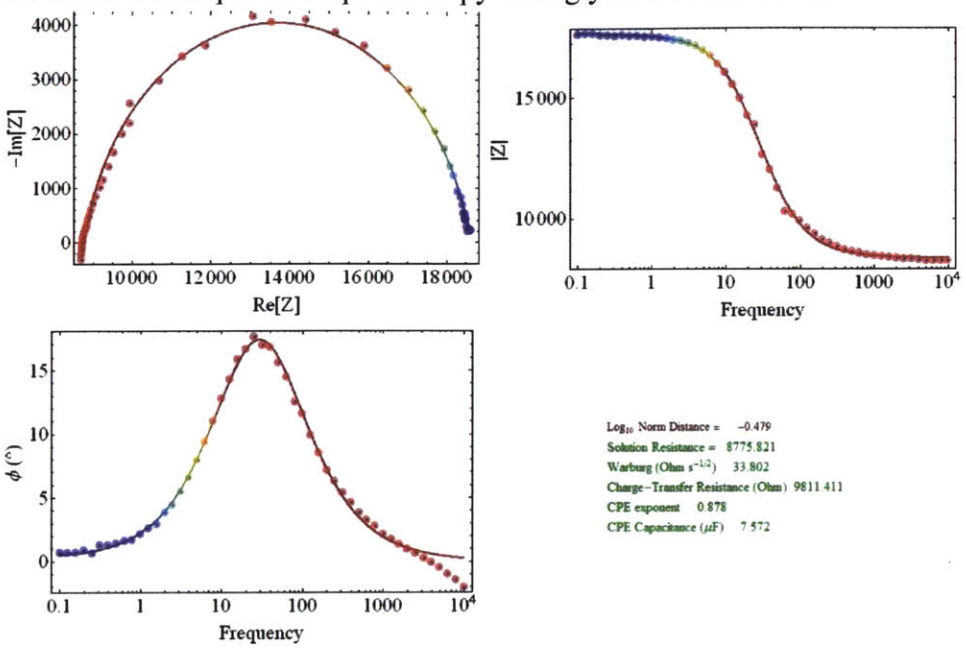

1.1.8 Electrochemical Impedance Spectroscopy Tetraglyme Calculation

Sulfur Conc. (Molar)	Ionic Cond. (mS/cm)	Solution Resist. (Ohm)	Warburg (Ohm s-1)	Charge-Transfer Resist (Ohm)
1	2.12	823.9	-60.1	19759
2.5	1.626	1204.3	-29.7	10539
3	1.518	1157.0	-16.3	11468
4	1.106	1625.5	-2.3	11074
5	0.769	2455.7	29.3	7184
7	0.264	5249.2	13.4	10228
8	0.161	8775.8	33.8	9811
Sulfur Conc. (Molar)	CPE Exponent	CPE Capacitance (uF)	Exchange Current (mA/s)	Exchange Current Density (mA/cm2 s)
1	0.896	8.76	0.00131	0.0185
2.5	0.891	10.77	0.00245	0.0347
3	0.884	9.89	0.00225	0.0319
4	0.885	10.16	0.00233	0.0330
5	0.866	11.06	0.00360	0.0509
7	0.887	8.29	0.00253	0.0358
8	7.572	7.57	0.00263	0.0373

1.2 Electrochemical Impedance Spectroscopy Diglyme

1.2.1 Electrochemical Impedance Spectroscopy Diglyme 1 Molar Sulfur

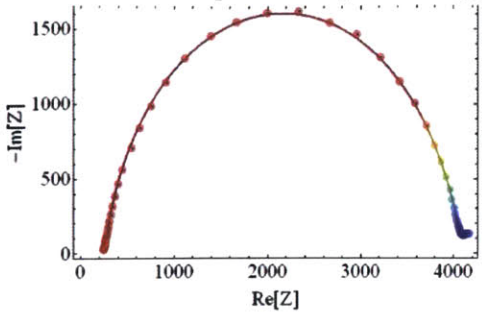

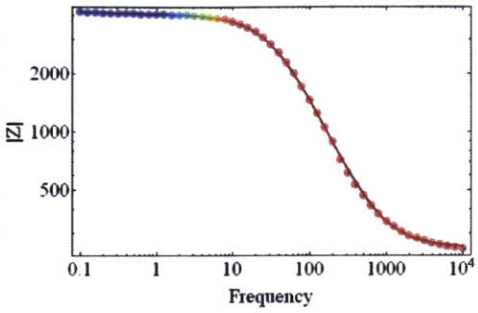

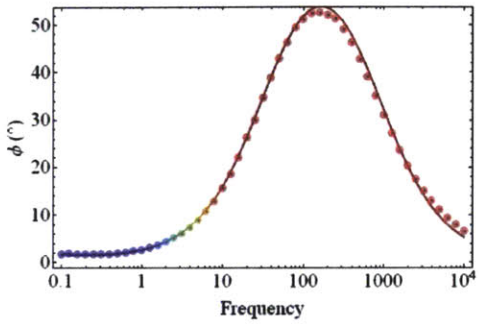

Log_{10} Norm Distance = −0.578
Solution Resistance = 252.690
Warburg (Ohm $s^{-1/2}$) 46.689
Charge−Transfer Resistance (Ohm) 3811.632
CPE exponent 0.892
CPE Capacitance (μF) 11.031

1.2.2 Electrochemical Impedance Spectroscopy Diglyme 2.5 Molar Sulfur

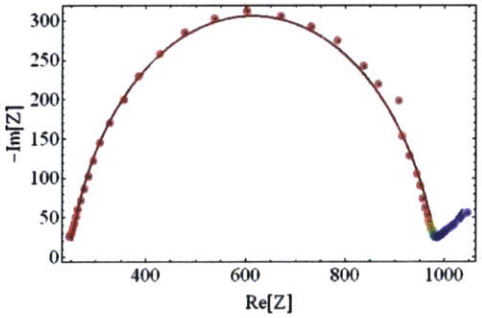

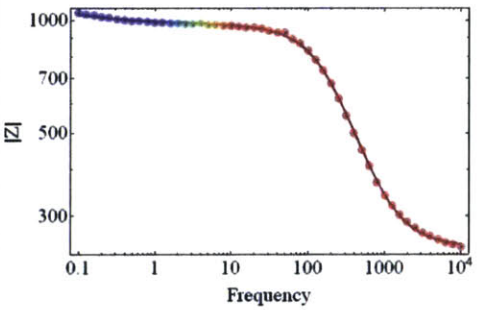

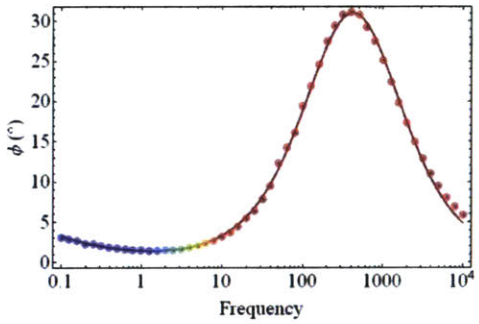

Log_{10} Norm Distance = −0.431
Solution Resistance = 247.243
Warburg (Ohm $s^{-1/2}$) 26.236
Charge−Transfer Resistance (Ohm) 729.990
CPE exponent 0.888
CPE Capacitance (μF) 12.726

1.2.3 Electrochemical Impedance Spectroscopy Diglyme 3 Molar Sulfur

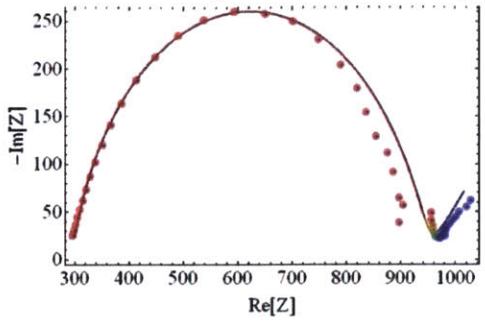

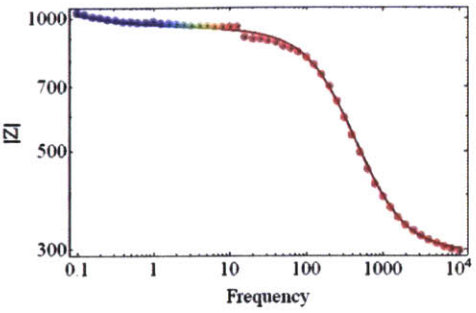

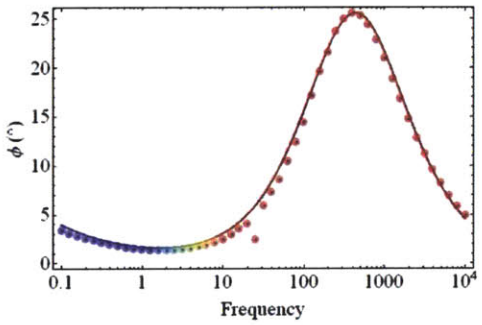

Log_{10} Norm Distance = −0.559
Solution Resistance = 294.034
Warburg (Ohm $s^{-1/2}$) 31.187
Charge−Transfer Resistance (Ohm) 652.548
CPE exponent 0.857
CPE Capacitance (μF) 14.932

1.2.4 Electrochemical Impedance Spectroscopy Diglyme 4 Molar Sulfur

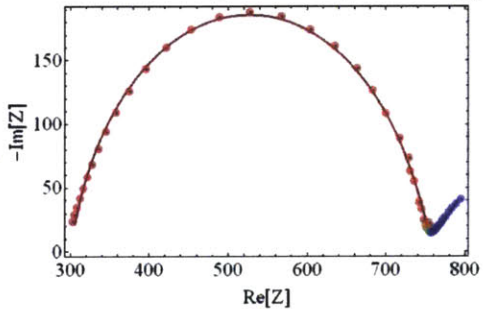

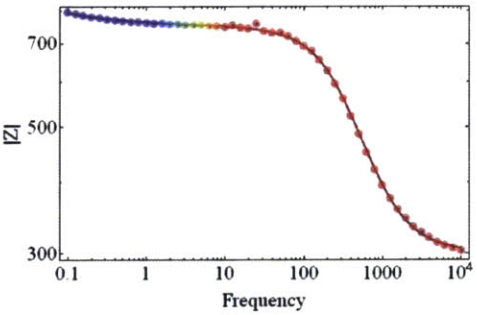

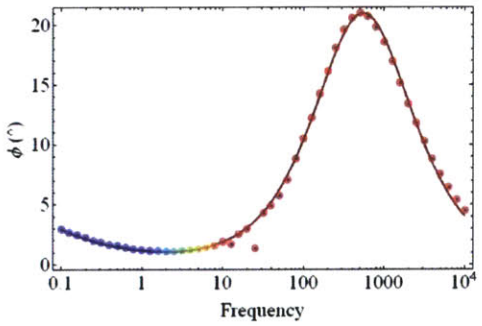

Log_{10} Norm Distance = −0.415
Solution Resistance = 300.913
Warburg (Ohm $s^{-1/2}$) 17.971
Charge−Transfer Resistance (Ohm) 450.796
CPE exponent 0.877
CPE Capacitance (μF) 13.881

1.2.5 Electrochemical Impedance Spectroscopy Diglyme 5 Molar Sulfur

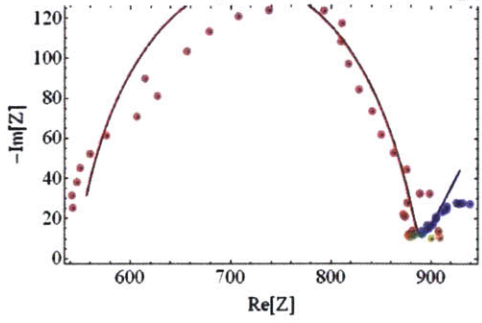

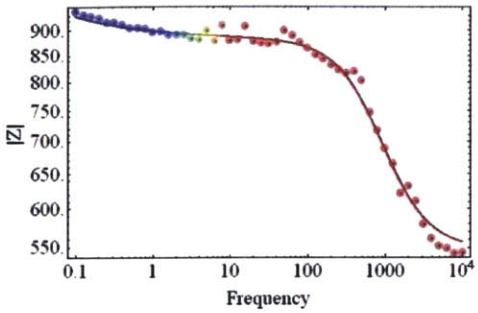

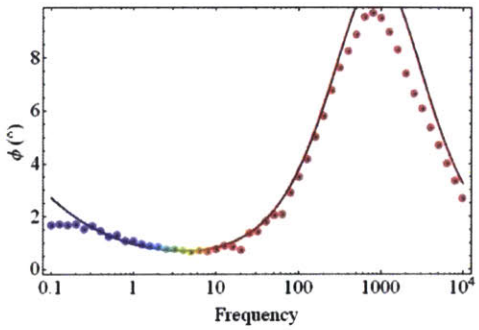

Log_{10} Norm Distance = −0.607
Solution Resistance = 546.344
Warburg (Ohm $s^{-1/2}$) 19.641
Charge−Transfer Resistance (Ohm) 338.848
CPE exponent 0.866
CPE Capacitance (μF) 10.136

1.2.6 Electrochemical Impedance Spectroscopy Diglyme 6 Molar Sulfur

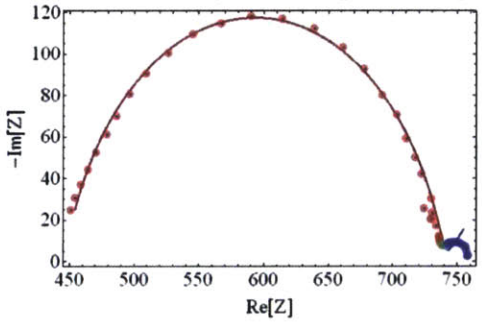

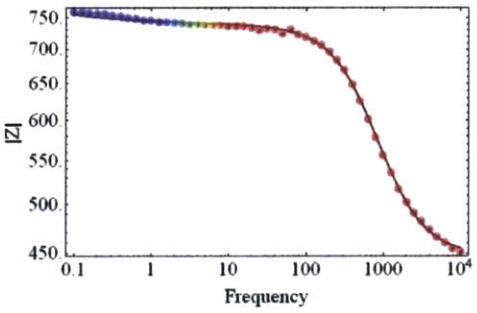

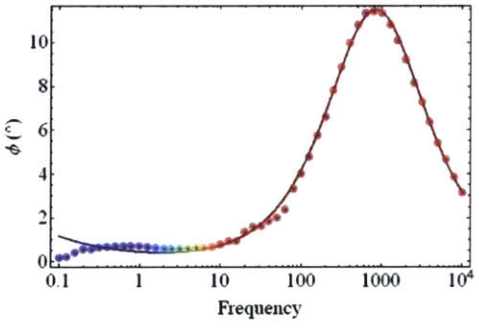

Log_{10} Norm Distance = −0.370
Solution Resistance = 446.381
Warburg (Ohm $s^{-1/2}$) 6.822
Charge−Transfer Resistance (Ohm) 293.336
CPE exponent 0.859
CPE Capacitance (μF) 13.415

1.2.7 Electrochemical Impedance Spectroscopy Diglyme 8 Molar Sulfur

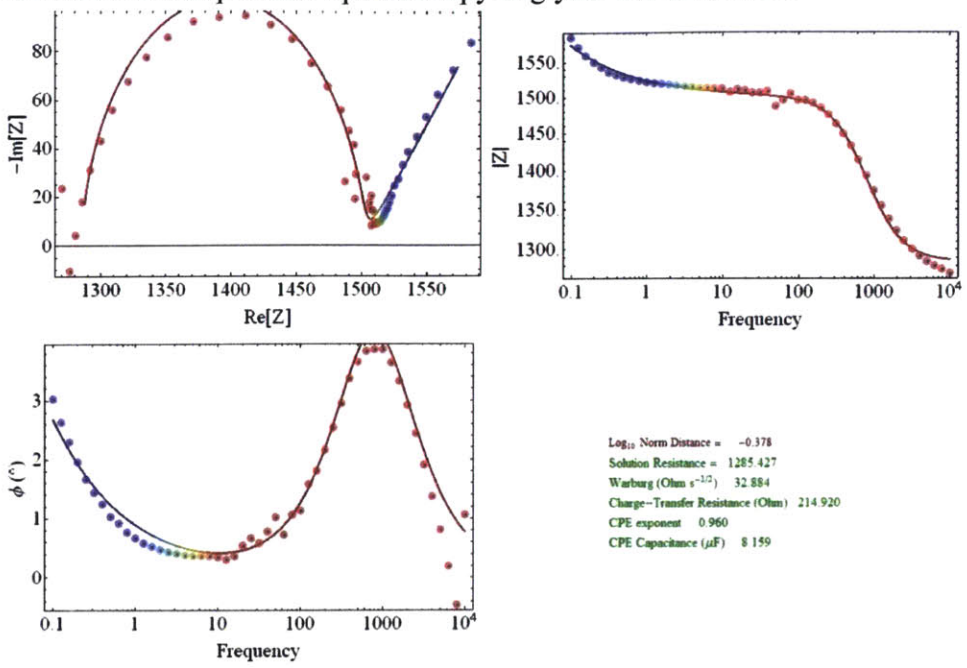

1.2.8 Electrochemical Impedance Spectroscopy Diglyme Calculation

Sulfur Conc. (Molar)	Ionic Cond. (mS/cm)	Solution Resist. (Ohm)	Warburg (Ohm s-1)	Charge-Transfer Resist (Ohm)
1	6.47	252.7	46.7	3811.6
2.5	6.02	247.2	26.2	730.0
3	5.81	294.0	31.2	652.5
4	5.38	300.9	18.0	450.8
5	4.89	546.3	19.6	338.9
6	4.00	446.4	6.8	293.3
8	2.27	1285.4	32.9	214.9
Sulfur Conc. (Molar)	CPE Exponent	CPE Capacitance (uF)	Exchange Current (mA/s)	Exchange Current Density (mA/cm2 s)
1	0.892	11.03	0.00678	0.0959
2.5	0.888	12.73	0.03541	0.5010
3	0.857	14.93	0.03961	0.5604
4	0.877	13.88	0.05734	0.8113
5	0.866	10.15	0.07628	1.0791
6	0.859	13.42	0.08813	1.2467
8	0.96	8.16	0.12028	1.7016

1.3 Electrochemical Impedance Spectroscopy DOL:DME

1.3.1 Electrochemical Impedance Spectroscopy DOL:DME 1 Molar Sulfur

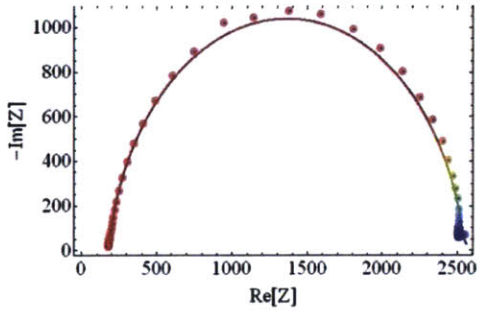

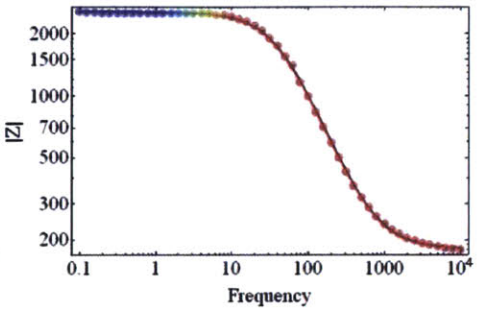

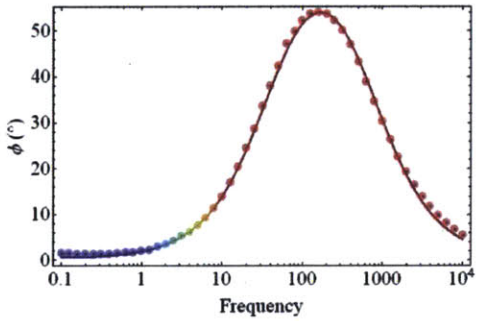

Log_{10} Norm Distance = −0.561
Solution Resistance = 181.017
Warburg (Ohm $s^{-1/2}$) 8.951
Charge−Transfer Resistance (Ohm) 2364.840
CPE exponent 0.918
CPE Capacitance (μF) 14.260

1.3.2 Electrochemical Impedance Spectroscopy DOL:DME 2.5 Molar Sulfur

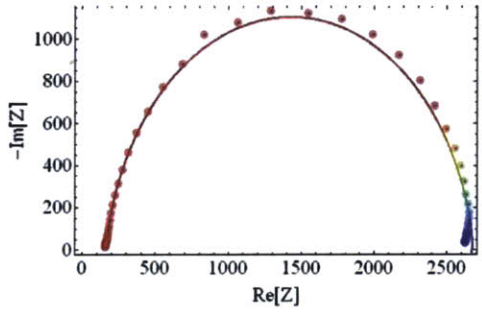

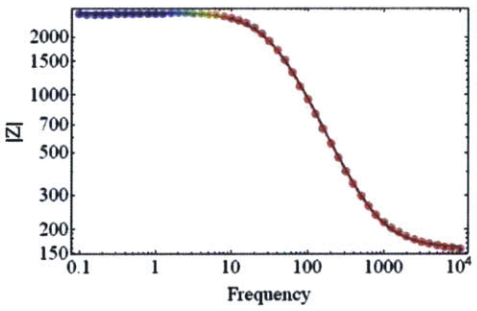

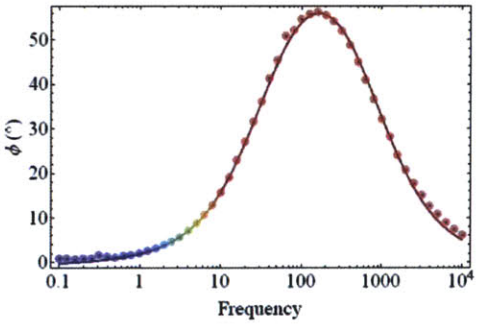

Log_{10} Norm Distance = −0.578
Solution Resistance = 159.749
Warburg (Ohm $s^{-1/2}$) −9.879
Charge−Transfer Resistance (Ohm) 2533.069
CPE exponent 0.914
CPE Capacitance (μF) 15.331

1.3.3 Electrochemical Impedance Spectroscopy DOL:DME 4 Molar Sulfur

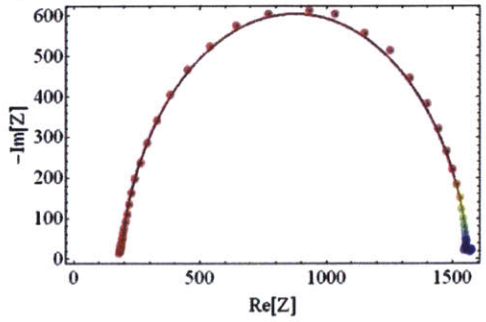

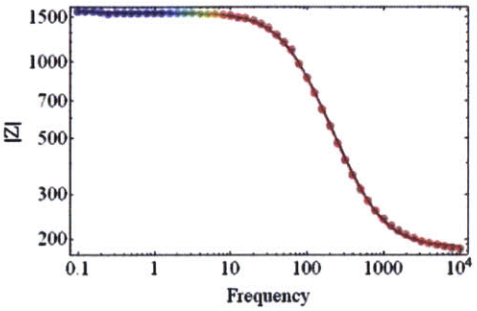

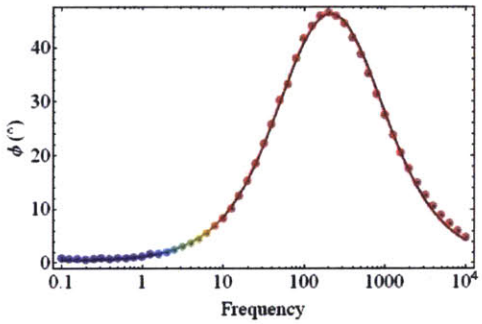

Log_{10} Norm Distance = −0.481
Solution Resistance = 184.719
Warburg (Ohm $s^{-1/2}$) 4.516
Charge−Transfer Resistance (Ohm) 1380.615
CPE exponent 0.915
CPE Capacitance (μF) 15.656

1.3.4 Electrochemical Impedance Spectroscopy DOL:DME 5 Molar Sulfur

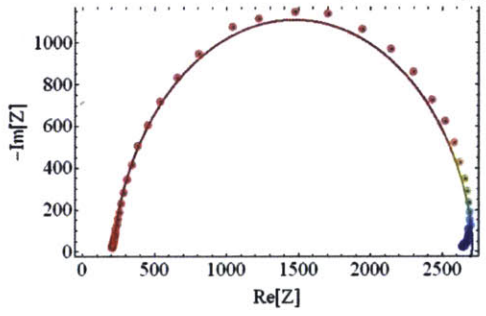

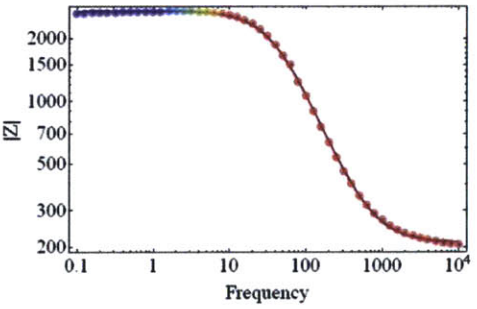

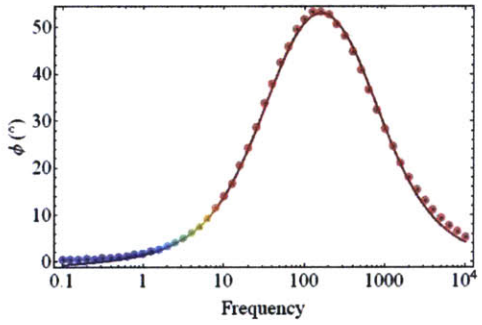

Log_{10} Norm Distance = −0.602
Solution Resistance = 209.147
Warburg (Ohm $s^{-1/2}$) −19.669
Charge−Transfer Resistance (Ohm) 2524.932
CPE exponent 0.919
CPE Capacitance (μF) 13.441

1.3.5 Electrochemical Impedance Spectroscopy DOL:DME 6 Molar Sulfur

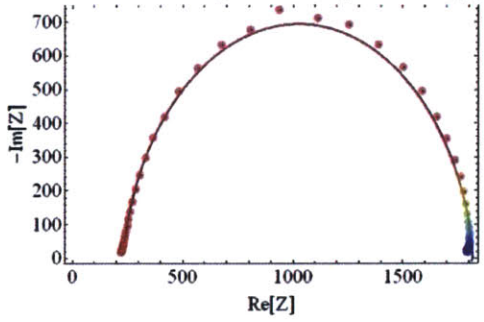

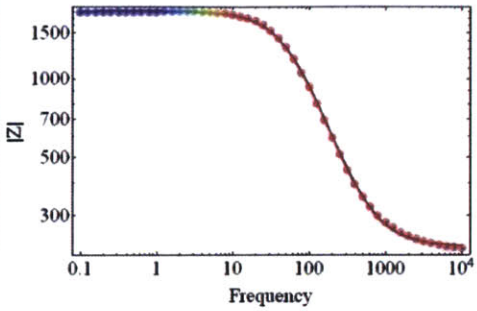

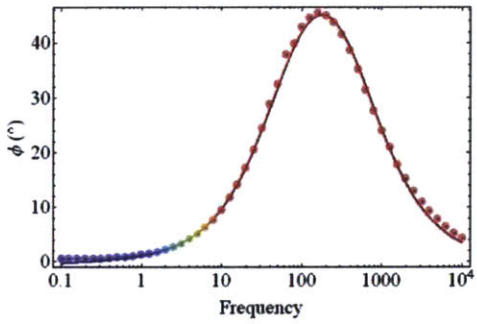

Log_{10} Norm Distance = −0.538
Solution Resistance = 227.641
Warburg (Ohm $s^{-1/2}$) −5.737
Charge−Transfer Resistance (Ohm) 1599.233
CPE exponent 0.910
CPE Capacitance (μF) 15.794

1.3.6 Electrochemical Impedance Spectroscopy DOL:DME 8 Molar Sulfur

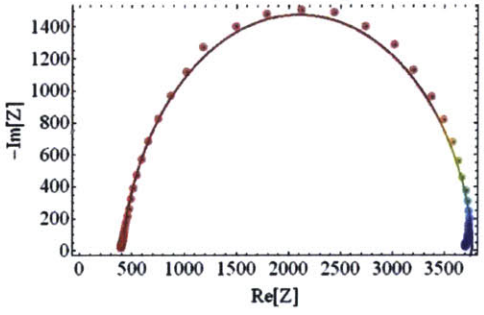

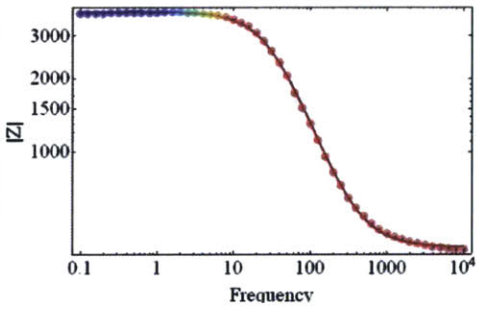

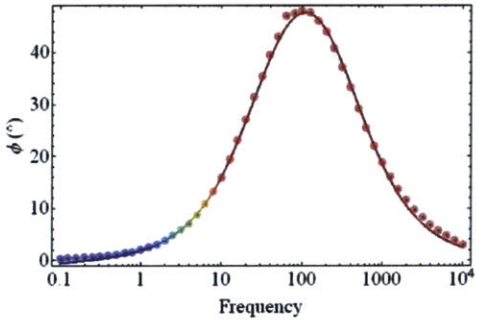

Log_{10} Norm Distance = −0.551
Solution Resistance = 403.197
Warburg (Ohm $s^{-1/2}$) −23.855
Charge−Transfer Resistance (Ohm) 3398.740
CPE exponent 0.911
CPE Capacitance (μF) 12.600

1.3.7 Electrochemical Impedance Spectroscopy DOL:DME Calculation

Sulfur Conc. (Molar)	Ionic Cond. (mS/cm)	Solution Resist. (Ohm)	Warburg (Ohm s-1)	Charge-Transfer Resist (Ohm)
1	9.29	181.02	9.0	2365
2.5	9.07	159.75	-9.9	2533
4	8.42	184.72	4.5	1381
5	7.08	209.15	-19.7	2525
6	6.02	227.64	-5.7	1599
8	3.72	403.20	-23.9	3399
Sulfur Conc. (Molar)	CPE Exponent	CPE Capacitance (uF)	Exchange Current (mA/s)	Exchange Current Density (mA/cm2 s)
1	0.918	14.26	0.01093	0.1546
2.5	0.914	15.33	0.01021	0.1444
4	0.915	15.66	0.01872	0.2649
5	0.919	13.44	0.01024	0.1448
6	0.91	15.79	0.01616	0.2287
8	0.911	12.60	0.00761	0.1076

Appendix 2. Solution Resistance in Different Solvent System

1.4 Solution Resistance versus Concentration in Tetraglyme

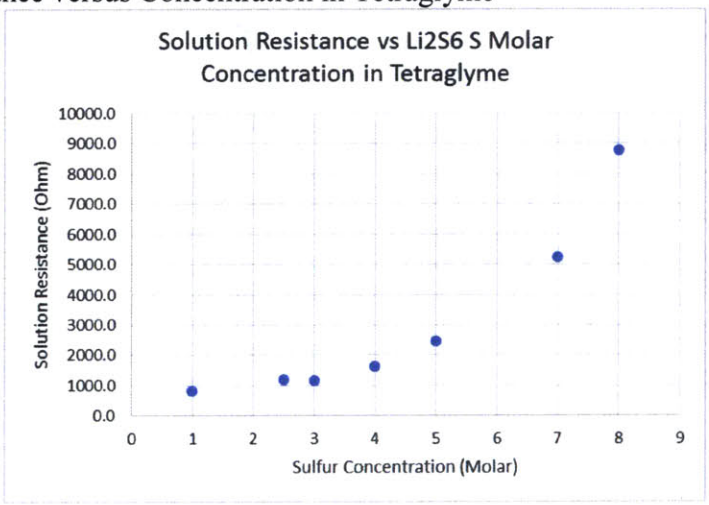

1.5 Solution Resistance versus Concentration in Triglyme

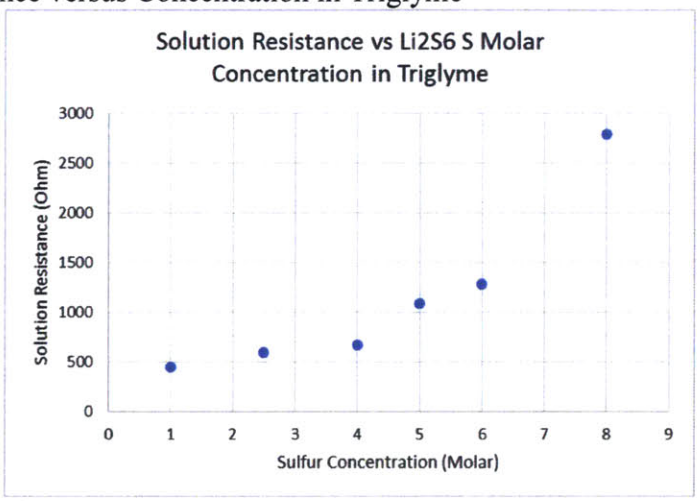

1.6 Solution Resistance versus Concentration in Diglyme

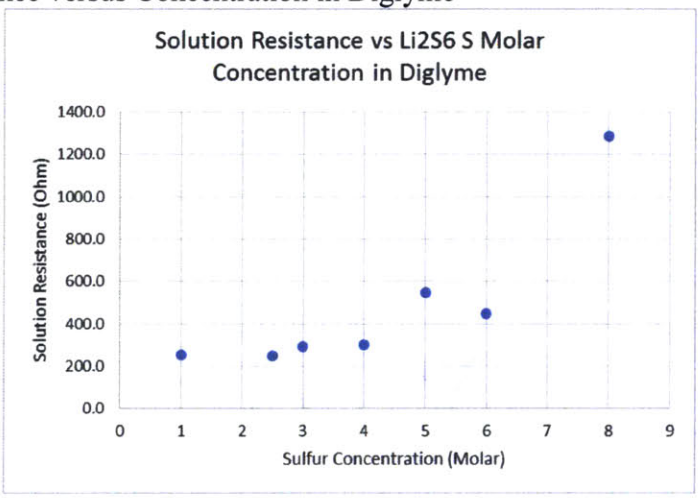

1.7 Solution Resistance versus Concentration in DOL:DME

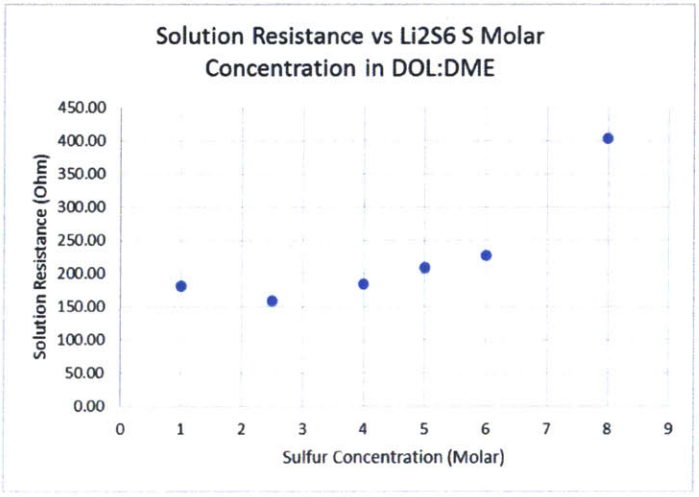

Appendix 3. Galvanostatic Polarization for Varying Concentration in Different Solvent System

3.1 Galvanostatic Polarization Tetraglyme

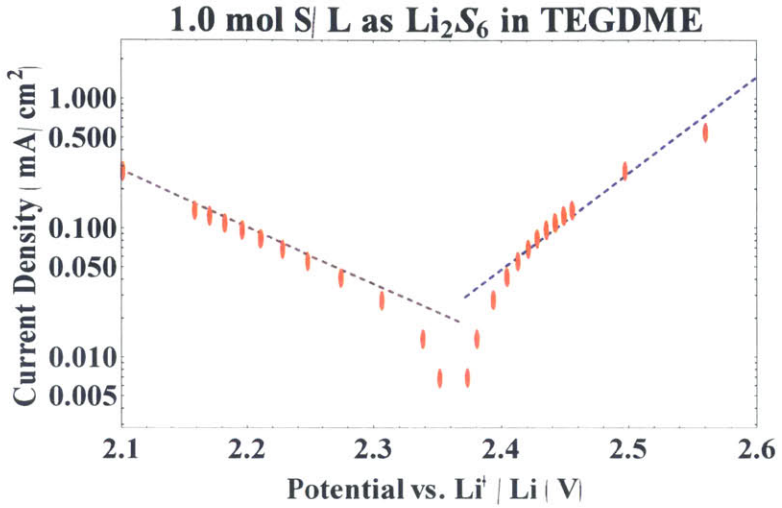

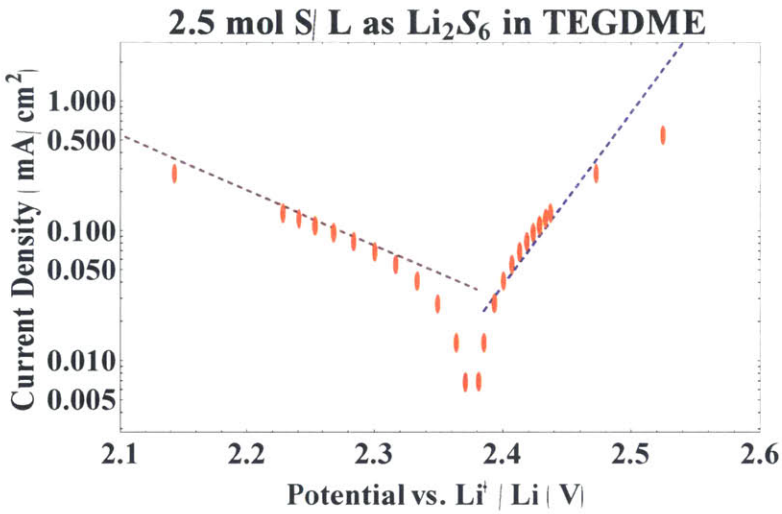

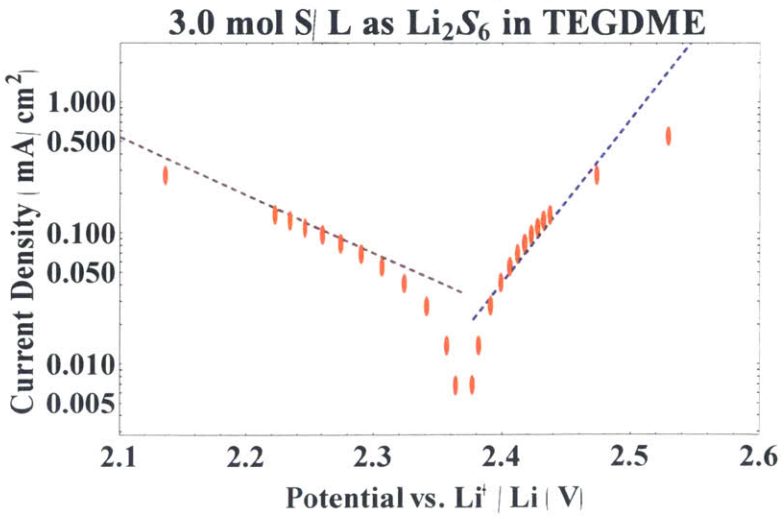

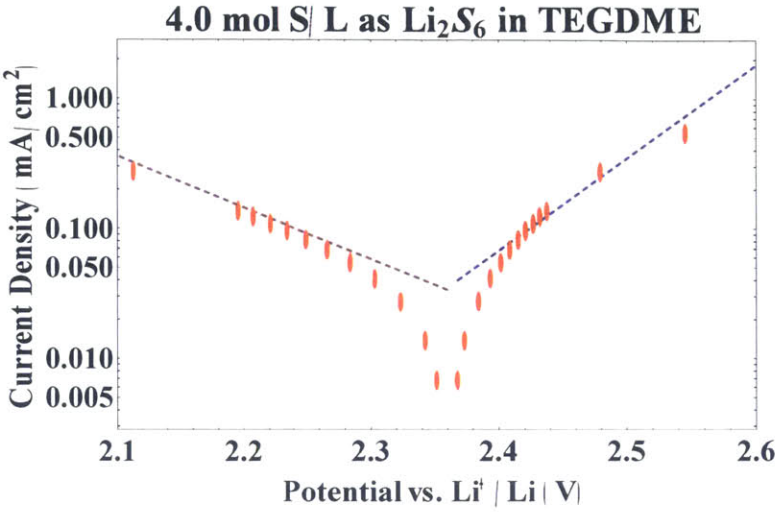
4.0 mol S/ L as Li_2S_6 in TEGDME
Current Density (mA/ cm^2)
1.000
0.500
0.100
0.050
0.010
0.005
2.1
2.2
2.3
2.4
2.5
2.6
Potential vs. Li$^+$ / Li (V)

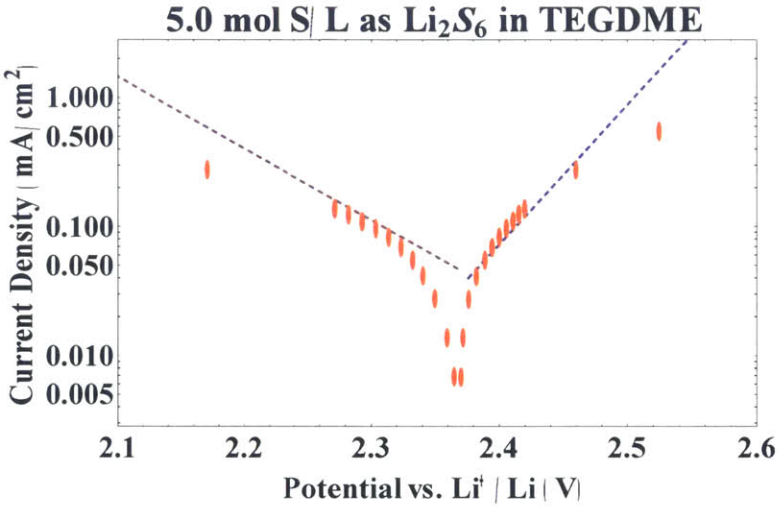
5.0 mol S/ L as Li_2S_6 in TEGDME
Current Density (mA/ cm^2)
1.000
0.500
0.100
0.050
0.010
0.005
2.1
2.2
2.3
2.4
2.5
2.6
Potential vs. Li$^+$ / Li (V)

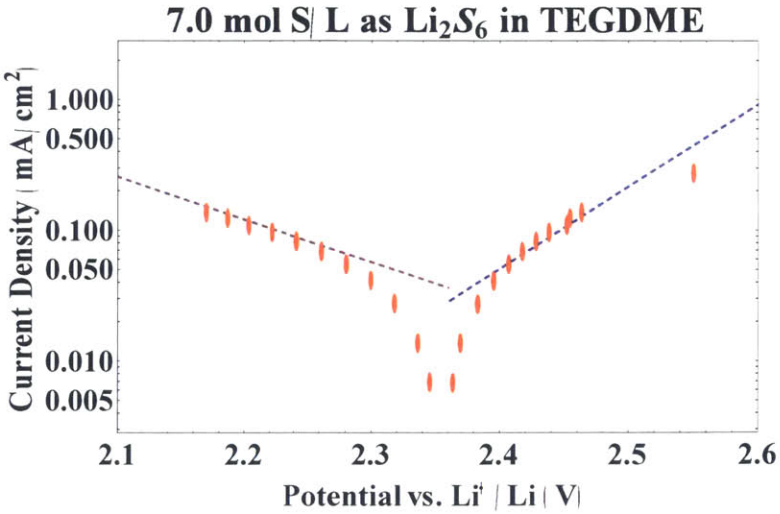
7.0 mol S/ L as Li_2S_6 in TEGDME
Current Density (mA/ cm^2)
1.000
0.500
0.100
0.050
0.010
0.005
2.1
2.2
2.3
2.4
2.5
2.6
Potential vs. Li$^+$ / Li (V)

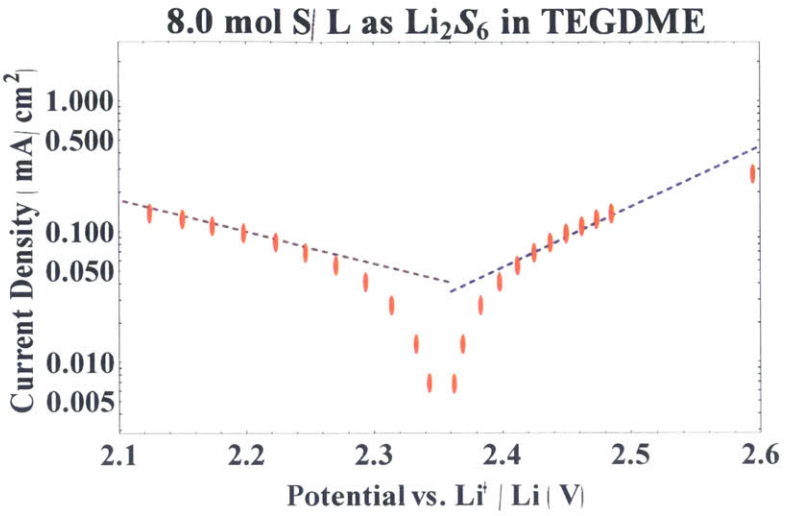

3.1.1 Tetraglyme Exchange Current Density from Galvanostatic Polarization

Sulfur Conc. (Molar)	Exchange Current Density (mA/cm2 s)
1	0.0228
2.5	0.0334
3	0.0351
4	0.0355
5	0.0395
7	0.0389
8	0.0376

3.2 Galvanostatic Polarization Triglyme

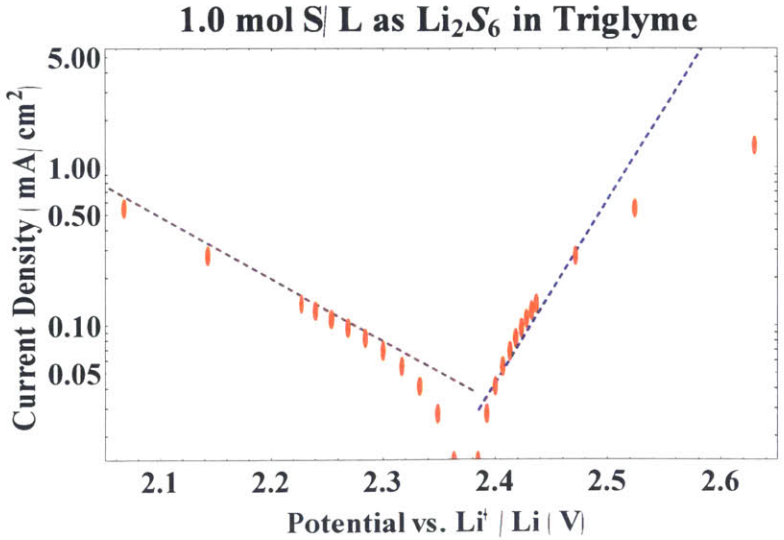

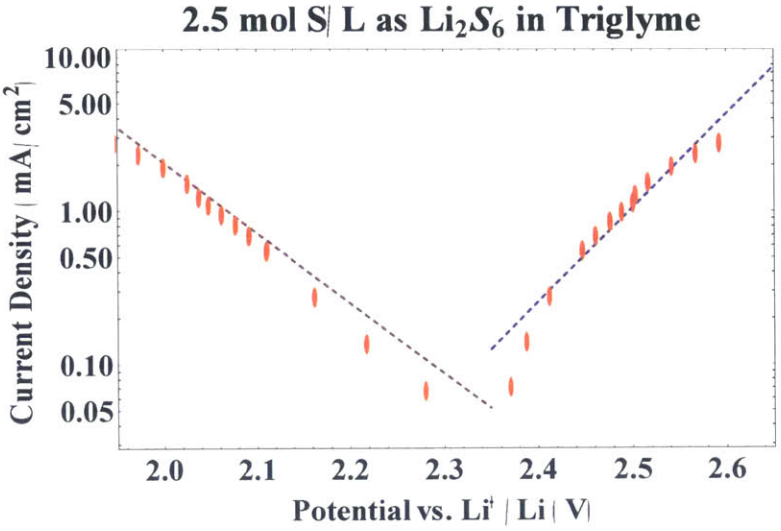
2.5 mol S/ L as Li_2S_6 in Triglyme
Current Density (mA/ cm^2)
10.00
5.00
1.00
0.50
0.10
0.05
2.0
2.1
2.2
2.3
2.4
2.5
2.6
Potential vs. Li$^+$ / Li (V)

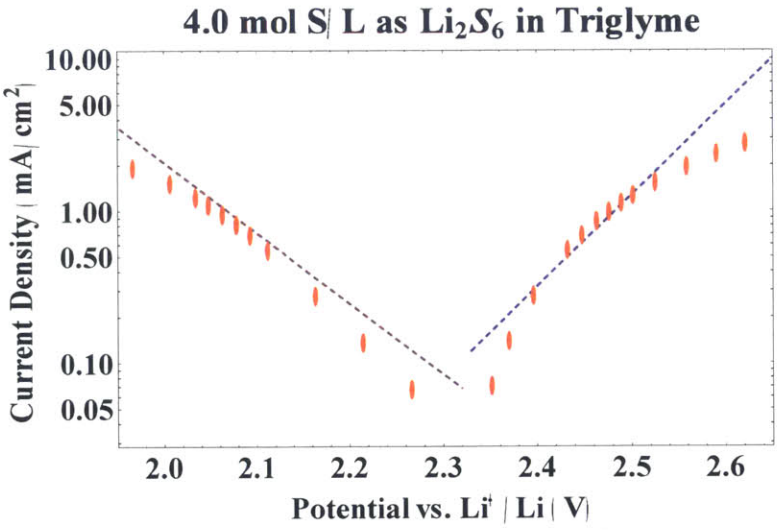
4.0 mol S/ L as Li_2S_6 in Triglyme
Current Density (mA/ cm^2)
10.00
5.00
1.00
0.50
0.10
0.05
2.0
2.1
2.2
2.3
2.4
2.5
2.6
Potential vs. Li$^+$ / Li (V)

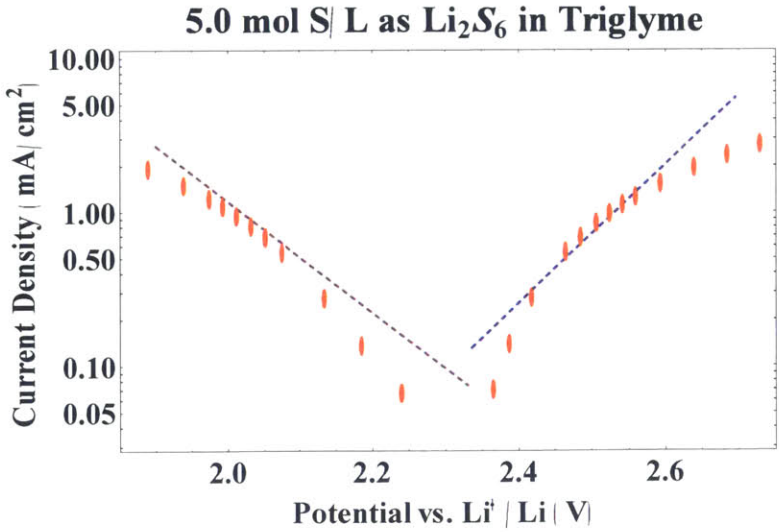
5.0 mol S/ L as Li_2S_6 in Triglyme
Current Density (mA/ cm^2)
10.00
5.00
1.00
0.50
0.10
0.05
2.0
2.2
2.4
2.6
Potential vs. Li$^+$ / Li (V)

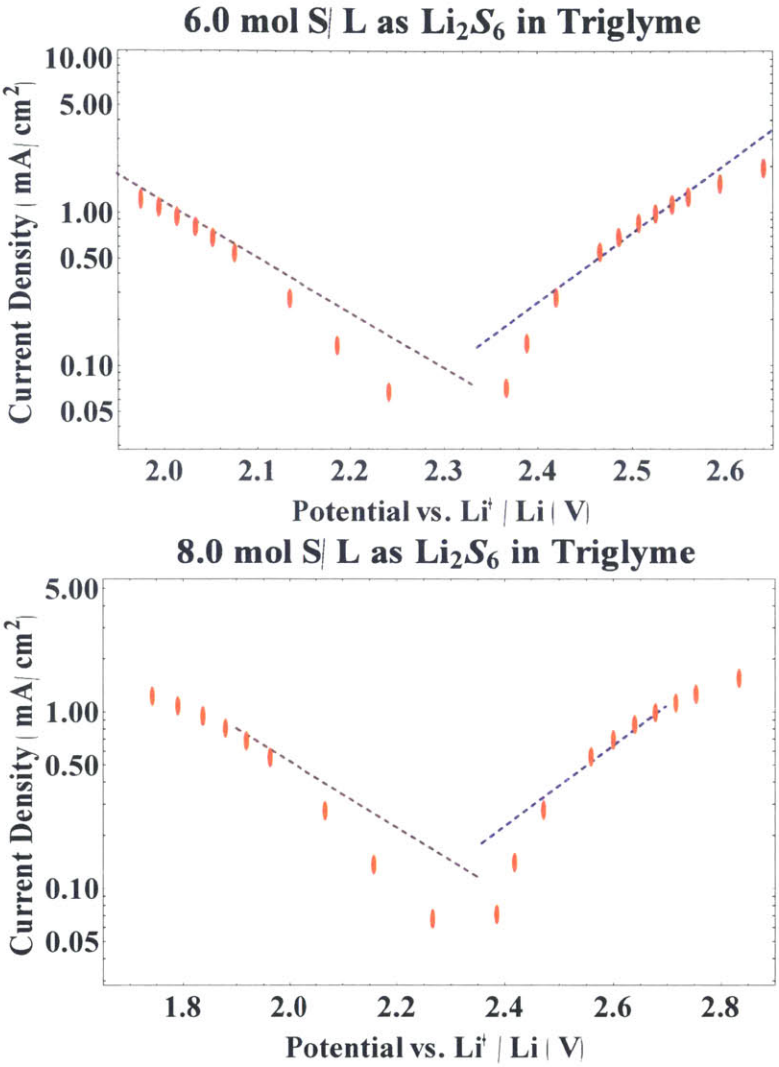

3.2.1 Triglyme Exchange Current Density from Galvanostatic Polarization

Sulfur Conc. (Molar)	Exchange Current Density (mA/cm2 s)
1	0.0732
2.5	0.0807
4	0.0859
5	0.0974
6	0.1015
8	0.1103

3.3 Galvanostatic Polarization Diglyme

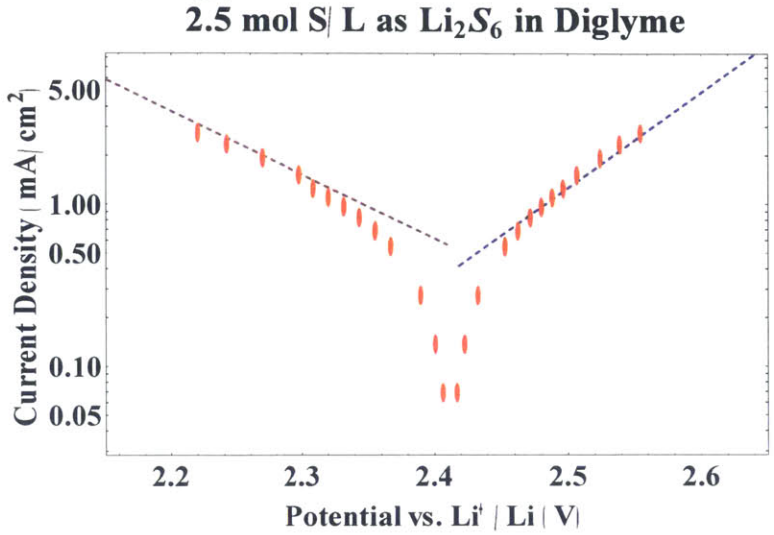

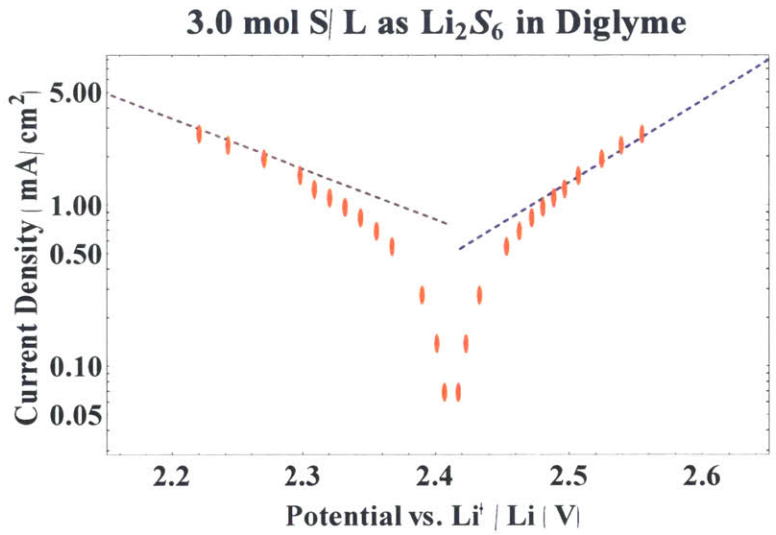

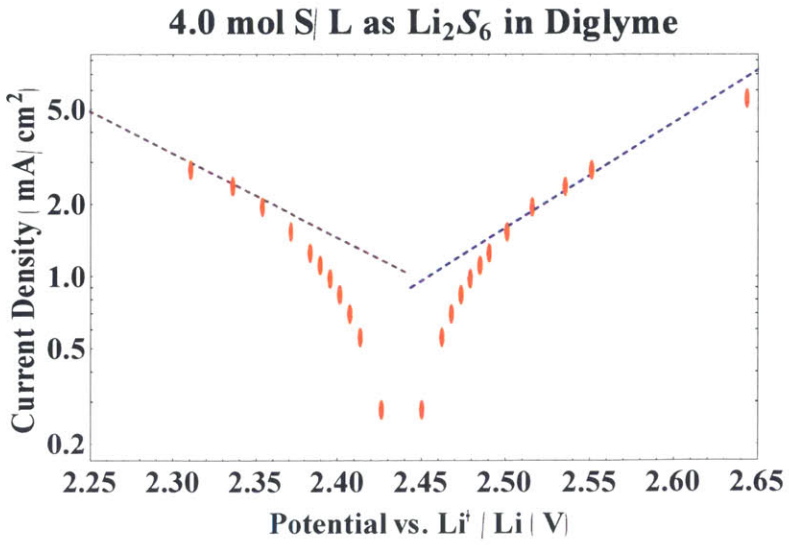

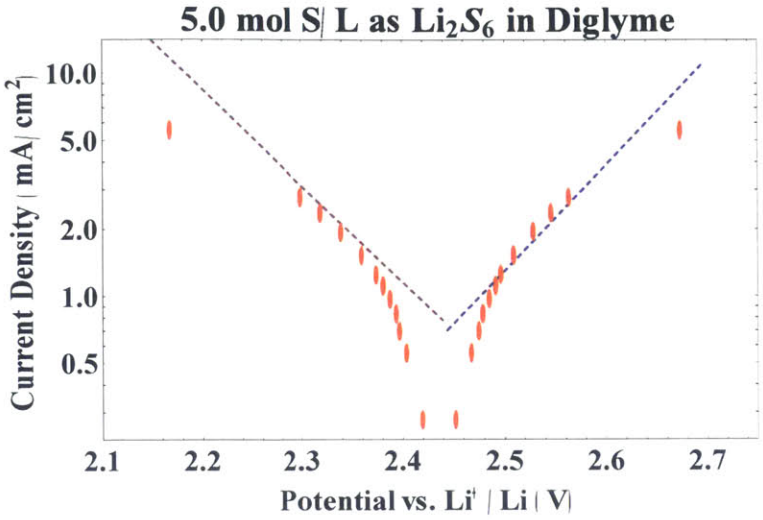

3.3.1 Diglyme Exchange Current Density from Galvanostatic Polarization

Sulfur Conc. (Molar)	Exchange Current Density (mA/cm2 s)
2.5	0.467
3	0.696
4	0.956
5	1.145